

**CONTROLS ON ISOTOPIC AND ELEMENTAL INCORPORATION OF LITHIUM IN
INORGANIC CALCIUM CARBONATES**

A THESIS SUBMITTED TO THE GRADUATE DIVISION OF THE UNIVERSITY OF
HAWAI'I AT MĀNOA IN PARTIAL FULFILLMENT OF THE REQUIREMENTS FOR THE
DEGREE OF

MASTER OF SCIENCE
IN
OCEANOGRAPHY
AUGUST 2023

By,
Corinne G. Hite

Thesis Committee:

Joji Uchikawa, Chairperson
Brian Popp
Malte Stuecker
Richard E. Zeebe

Keywords: isotopic geochemistry, lithium, paleoceanography

ACKNOWLEDGEMENTS

This thesis is the result of a collaborative effort, with contributions from multiple people at various institutions across the globe.

A significant amount of the analysis work was conducted at the Indian Institute of Science, Bangalore with direction from Dr. Sambuddha Misra. Sample analysis was conducted by Satya Chanakya, Pratyusha Chanda, and Neha Tanwar. I would also like to acknowledge Dr. Sajeev Krishnan and Pranaykumar Tirpude for their assistance.

Maintenance of the pH-stat system used in experiments was provided by Dr. Chris Langdon at the University of Miami and additional sample analysis was conducted by Dr. James Zachos and Xiaodong Daisy Zhang at the University of California, Santa Cruz.

There are many people at the University of Hawai‘i at Mānoa who were instrumental in this research study, including Dr. Jian Yu and Dr. Phuong Nguyen. I would like to especially acknowledge my advisor Dr. Joji Uchikawa, Dr. Richard Zeebe, Dr. Malte Stuecker, and Dr. Brian Popp for their guidance. I would also like to acknowledge the contributions of the staff in the Oceanography Office, namely Van Tran, Kristin Momohara, and Kellie Terada.

Lastly, I would like to thank my family and friends for their support and encouragement.

ABSTRACT

There is increasing interest in using the $\delta^7\text{Li}$ value of marine biogenic CaCO_3 (i.e., foraminifera tests) as a tracer for secular changes in silicate weathering, an important process in sequestering atmospheric CO_2 . However, culture studies have suggested the possibility of additional controls on Li incorporation in foraminiferal CaCO_3 , indicating a need to better understand the physical and chemical controls on Li incorporation in inorganic CaCO_3 without the complications of vital effects from a biological system. To this end, the present study conducted inorganic calcite and aragonite precipitation experiments with systematic manipulations of solution chemistry parameters (pH, [DIC], and $[\text{Ca}^{2+}]$) using a pH-stat system. Both calcite and aragonite samples had lower $\delta^7\text{Li}$ values than the $\delta^7\text{Li}$ value of dissolved Li in the experimental solution, indicating preferential uptake of the lighter isotope (^6Li) in carbonate minerals. This is presumably due to the tetrahedral coordination of Li bound with water molecules in solution resulting in the strongest bonds. Aragonite consistently had $\delta^7\text{Li}$ values lower than calcite, likely due to differences in Li coordination within the crystal lattice and the resulting bond strength. There was an observed effect on the Li isotopic fractionation in aragonite samples with changes in pH, [DIC], and $[\text{Ca}^{2+}]$. Additionally, a significant relationship was found between the Li isotopic fractionation in calcite samples and pH. Despite being statistically significant, these relationships were weak and resulted in a minimal overall effect on fractionation compared to the experimental uncertainty. There was no clear relationship observed between precipitation rate and fractionation, suggesting fractionation is dominated by equilibrium effects rather than kinetic effects. Overall, the present study has implications for the use of Li in carbonate minerals as a proxy tool for silicate weathering. In particular, while precipitation rate and solution chemistry may not dramatically influence Li isotope fractionation

in inorganic calcite, biological vital effects may play a significant role and should be further evaluated in order to confidently use Li isotopes for silicate weathering reconstructions.

TABLE OF CONTENTS

Acknowledgements.....	i
Abstract.....	ii
List of Tables.....	v
List of Figures.....	vi
Thesis.....	1
1. Introduction.....	1
2. Methods.....	6
2.1 Overview.....	6
2.2 Experimental Design.....	8
2.3 Preparation of Stock Solutions.....	11
2.4 Preparation & Characterization of CaCO ₃ Seeds.....	12
2.5 ¹³ C Mass Balance.....	13
2.6 Analytical Methods.....	14
2.6.1 δ ¹³ C Analysis.....	14
2.6.2 Elemental Analysis.....	14
2.6.3 δ ⁷ Li Analysis.....	15
3. Results.....	16
3.1 Visual & Mineralogical Characterization of CaCO ₃ Seeds.....	16
3.2 Trial Experiments.....	16
3.3 Experimental Solution & Parameter Manipulation.....	18
3.4 Elemental & Isotopic Composition of Samples.....	29
4. Discussion.....	23
4.1 Li Isotope Fractionation in Inorganic Calcite vs. Aragonite.....	23
4.2 Controls on Li Isotopic Fractionation in CaCO ₃ with Respect to Solution.....	27
4.2.1 Calcite.....	27
4.2.2 Aragonite.....	31
4.3 Controls on Li/Ca.....	31
4.4 Effects of Mg ²⁺ on Precipitation.....	34
4.5 Comparison with Culture Experiments.....	35
5. Summary & Conclusions.....	37
Appendix.....	40
References.....	50

LIST OF TABLES

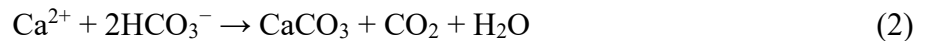
Table 1: Summary of Manipulations and Experimental Solution.....	10
Table 2: Calcite and Aragonite Seed Characteristics.....	13
Table 3: Statistical Analysis.....	22
Table A1: $\delta^{13}\text{C}$ and $\delta^{18}\text{O}$ values of BaCO_3 samples (Appendix).....	40
Table A2: Experimental Solution Concentrations (Appendix).....	40
Table A3: $\delta^7\text{Li}$, ${}^7\varepsilon_{\text{solid-solution}}$, and $\text{Log}R$ Data (Appendix).....	42
Table A4: Li/Ca and D_{Li} Data (Appendix).....	43
Table A5: Na/Ca and Mg/Ca Data (Appendix).....	45

LIST OF FIGURES

Figure 1: Sources and Sinks of Li to Ocean.....	2
Figure 2: Experimental Set Up.....	7
Figure 3: pH-Stat System Titration Plot.....	8
Figure 4: SEM Images of CaCO ₃ Samples.....	17
Figure 5: ⁷ ε _{solid-solution} and D _{Li} values, Individual Parameter Experiments.....	20
Figure 6: ⁷ ε _{solid-solution} and D _{Li} values, [Ca ²⁺]/pH Parameter Experiments.....	21
Figure 7: Relationship between LogR and ⁷ ε _{solid-solution} and D _{Li} values.....	22
Figure 8: Aragonite and Calcite Ca ²⁺ Coordination.....	26
Figure 9: Relationship Between Li Coordination and Isotopic Fractionation.....	27
Figure 10: <i>Füger et al. (2022)</i> Model.....	29
Figure 11: Mg/Ca vs Li/Ca	32
Figure A1: Raman Plots (Appendix).....	47
Figure A2: ⁷ ε _{solid-solution} Across Multiple Studies (Appendix).....	47
Figure A3: Titrant Addition Rate Acceleration (Appendix).....	48
Figure A4: Titrant Addition Plots for [Ca ²⁺]/pH Series (Appendix).....	48
Figure A5: Mole Fraction MgCO ₃ vs Log K.....	49

1. INTRODUCTION

The chemical weathering of silicate rocks occurs when carbon dioxide (CO₂) from the atmosphere dissolves in water to form carbonic acid (H₂CO₃), which then reacts with continental silicate rocks. This process delivers Ca²⁺ ions and dissolved inorganic carbon (DIC) via rivers to the ocean, where they are used to precipitate calcium carbonate (CaCO₃) minerals that are eventually buried in marine sediments (*Faure & Mensing, 2004*; also see a review by *Zeebe, 2012*). This can be described as:



Equation (1) shows that silicate weathering removes a net one mole of carbon (as CO₂) from the atmosphere and buries it as CaCO₃. The system is balanced with the addition of carbon to the atmosphere from the degassing of volcanoes and oxidation of organic matter, resulting in a cycling of carbon on a timescale of 10⁵ - 10⁶ years (*Berner & Caldeira, 1997*; *Zeebe, 2012*). It is thought that higher levels of atmospheric CO₂ result in an elevated global temperature and intensified hydrological cycle, which leads to intensified silicate weathering and greater continental runoff (*Walker et al., 1981*). Consequently, silicate weathering processes increase under higher levels of atmospheric CO₂ until the excess atmospheric carbon is sequestered and the system returns to steady state. This makes silicate weathering an important negative feedback against increasing atmospheric CO₂ concentration, which is critical in maintaining Earth's habitable climate as well as restoring it after major perturbation events (*Walker et al., 1981*; *Raymo et al., 1988*; *Broecker & Sanyal, 1998*; *Zeebe & Caldeira, 2008*).

Carbon cycle models predict that the atmospheric CO₂ emitted by fossil fuel burning will eventually be sequestered by silicate weathering over the course of hundreds of thousands of years (*Lenton & Britton, 2006*). However, uncertainties in the parameterization of weathering fluxes can make it difficult to predict the timing of this process over large timescales, which leads to different estimates for the rates of carbon removal (*Uchikawa & Zeebe, 2008*). The use of weathering processes in Earth system models could be improved by gaining insight on the history of silicate weathering and its relation to changes in Earth's climate system (*Caves et al., 2016*).

To this end, there is a growing interest in using lithium (Li) as a tool for studying silicate weathering by reconstructing the isotopic composition of lithium (δ⁷Li) in seawater. Here, δ⁷Li is

defined as the ratio of ${}^7\text{Li}$ to ${}^6\text{Li}$ of the sample relative to the ratio of the certified reference standard material NIST SRM 8545 (LSVEC) in per mil (‰) (Hathorne & James, 2006; Misra & Froelich, 2012):

$$\delta^7\text{Li} = \frac{\left(\frac{{}^7\text{Li}}{{}^6\text{Li}}\right)_{\text{Sample}} - \left(\frac{{}^7\text{Li}}{{}^6\text{Li}}\right)_{\text{LSVEC}}}{\left(\frac{{}^7\text{Li}}{{}^6\text{Li}}\right)_{\text{LSVEC}}} \times 10^3 \quad (3)$$

The Li isotopic fractionation between a precipitating solid and the source solution (${}^7\varepsilon_{\text{solid-solution}}$) describes the relationship between the $\delta^7\text{Li}$ values of the two components, which is given by the following equation (Zeebe & Wolf-Gladrow, 2001):

$${}^7\varepsilon_{\text{solid-solut}} = \frac{(\delta^7\text{Li}_{\text{solid}} - \delta^7\text{Li}_{\text{solution}})}{1 + (\delta^7\text{Li}_{\text{solution}}/10^3)} \quad (4)$$

Li is conservative in seawater due to its high solubility and long residence time (10^6 years) compared to a much shorter timescale of ocean mixing (10^3 years). The major sources of Li in seawater are from rivers and hydrothermal vents, which are balanced by the removal of Li into sedimentary clays and altered basalts. (Chan et al., 1992; Huh et al., 1998). The magnitude of Li fluxes from hydrothermal and riverine sources are similar and on the order of 10^9 mol/year. However, $\delta^7\text{Li}$ values of these fluxes differ considerably (see **Figure 1**).

Hydrothermal vents have an average $\delta^7\text{Li}$ value of $\sim 8\%$. In contrast, the $\delta^7\text{Li}$ values of river waters can vary from 1 to 44‰ but have a global mean of $\sim 23\%$ (Pogge von Strandmann et

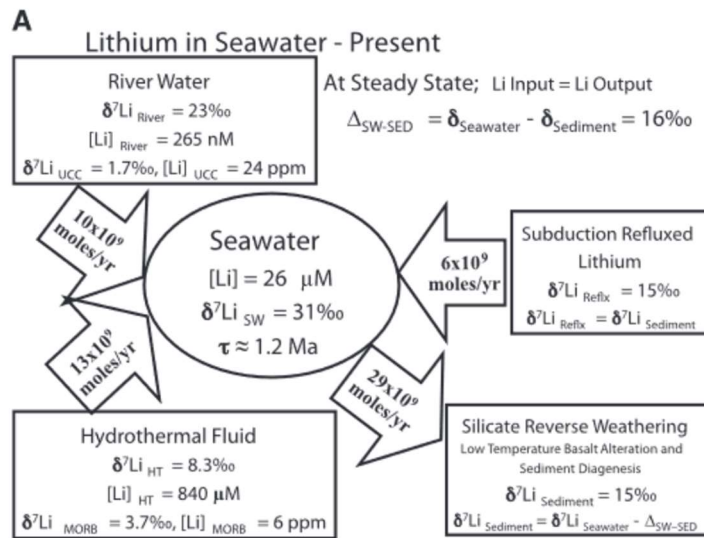


Figure 1: Sources and Sinks of Li to Ocean.

Diagram of balanced sources and sinks of Li to the modern ocean, their $\delta^7\text{Li}$ values and fluxes (Misra & Froelich, 2012).

al., 2013; *Penniston-Dorland et al.*, 2017). Modern seawater has a $\delta^7\text{Li}$ value of 31‰, which is relatively higher than the $\delta^7\text{Li}$ value of the hydrothermal and riverine Li sources to the ocean. Thus, the major sink of Li from the ocean is thought to be through alteration of oceanic crust and silicate reverse weathering, which is the incorporation of Li into sedimentary clays, a process that favors ^6Li over ^7Li (*Hathorne & James*, 2006; *Misra & Froelich*, 2012). Changes in seawater $\delta^7\text{Li}$ values over long timescales reflect an imbalance between these sources and sinks to the ocean, primarily driven by changes in silicate weathering and reverse weathering rates.

The large variability in riverine $\delta^7\text{Li}$ values is due to isotope fractionations related to formation of secondary clay minerals during chemical weathering of silicate rocks. The major control on the $\delta^7\text{Li}$ value of river water is the ratio of primary rock dissolution to the precipitation of secondary clay minerals. These clays favorably incorporate ^6Li , which results in river waters with comparatively higher $\delta^7\text{Li}$ values (*Huh et al.*, 1998; *Penniston-Dorland et al.*, 2017). Assuming that other sources and sinks of Li in seawater are relatively constant (*Hathorne & James*, 2006; *Li & West*, 2014), a strong coupling of the $\delta^7\text{Li}$ values of seawater and riverine sources can be expected. Under more intense weathering there is an increase in secondary clay mineral formation, driving riverine (and as a result, seawater) $\delta^7\text{Li}$ to higher values. Thus, changes in the $\delta^7\text{Li}$ value of seawater over prolonged periods of time can provide useful insight into silicate weathering throughout geologic history (*Hathorne & James*, 2006; *Misra & Froelich*, 2012; *Pogge von Strandmann et al.*, 2013).

$^{87}\text{Sr}/^{86}\text{Sr}$ and $^{187}\text{Os}/^{188}\text{Os}$ in marine CaCO_3 have also been proposed and used as silicate weathering proxies. However, the incorporation of osmium in shales and strontium in carbonates may result in mixed signals (*Ravizza & Zachos*, 2004; *Sun et al.*, 2018). In contrast, Li is almost exclusively found in silicate rocks with minimal incorporation in carbonates or shales. There is also no known influence on Li isotopes from biological processes such as plant uptake or primary production (*Misra & Froelich*, 2012; *Pogge von Strandmann et al.*, 2013; *Penniston-Dorland et al.*, 2017). This makes Li unique in exclusively tracing silicate processes, fueling the interest in using seawater $\delta^7\text{Li}$ values as a tracer for silicate weathering. Studies by *Marriott et al.* (2004a) and *Hall et al.* (2005) have shown that the $\delta^7\text{Li}$ values of modern foraminifera closely reflect the $\delta^7\text{Li}$ values of dissolved Li in modern seawater, suggesting that fossilized foraminifera can be used as a tracer for changes in seawater $\delta^7\text{Li}$ values in the past. Moreover, *Delaney et al.* (1985) and *Delaney & Boyle* (1986) showed good agreement between the Li/Ca

ratio of foraminifera and the Li/Ca ratio of seawater, implying Li/Ca ratios could provide additional insight into seawater Li geochemistry and the use of Li isotopes as a tracer for silicate weathering (*Hathorne & James, 2006; Stewart et al., 2017*).

However, more recent studies have identified the possibility of additional controls on the Li incorporation in biogenic CaCO₃, suggesting complications in using Li as a weathering proxy. Culture experiments by *Vigier et al. (2015)* tested the effect of changes in seawater pH and [DIC] on the $\delta^7\text{Li}$ value of a benthic foraminiferal species *Amphistegina lobifera*. While the study observed no significant relationship between $\delta^7\text{Li}$ and seawater pH, it noted a positive correlation between $\delta^7\text{Li}$ and [DIC]. Conversely, culture experiments using a different – but closely related – benthic foraminiferal species *Amphistegina lessonii* by *Roberts et al. (2018)* observed no significant effect on $\delta^7\text{Li}$ from [DIC], but a negative correlation between $\delta^7\text{Li}$ and pH. There have also been suggestions from core-top studies that some aspect of seawater dissolved carbonate chemistry controls Li/Ca ratios in CaCO₃ (*Lear et al., 2010*).

Ambiguous core-top and culture data from previous studies make it challenging to confidently use the $\delta^7\text{Li}$ value in fossilized foraminifera as a weathering proxy, as it is possible that the incorporation of Li in foraminifera tests is complicated by “vital effects” associated with a biological system. Vital effects refer to biases in paleo-proxies originating from physiological processes and cellular controls on the chemical composition of calcifying fluid from which these organisms secrete CaCO₃ (*de Nooijer et al. 2014*). This highlights a need to better understand the physical and chemical controls on Li incorporation in inorganic CaCO₃ without the complications of these vital effects.

Some studies have explored potential controls on $\delta^7\text{Li}$ values and Li distribution coefficient (D_{Li}) of inorganic CaCO₃ by several solution physicochemical parameters. Here, D_{Li} is defined as the Li/Ca ratio of the solid compared to that of the parent solution (*Marriott et al., 2004b*):

$$D_{\text{Li}} = ([\text{Li}]/[\text{Ca}]_{\text{solid}})/([\text{Li}]/[\text{Ca}]_{\text{solution}}) \quad (5)$$

Marriott et al. (2004b) tested the effect of temperature on Li incorporation in inorganic calcite. They observed no temperature dependence on the $\delta^7\text{Li}$ value of the samples but found an inverse relationship between temperature and D_{Li} . An additional study by *Marriott et al. (2004a)* focused on the relationship between salinity and Li incorporation in both inorganic calcite and aragonite. While they observed no significant relationship between salinity and the $\delta^7\text{Li}$ values of either

mineral, there was a larger isotope fractionation between CaCO_3 and parent solution for aragonite than calcite. The study also revealed a significant positive correlation between salinity and the D_{Li} value for calcite but not aragonite, indicating that CaCO_3 mineralogy may play a critical role in the incorporation of Li into CaCO_3 . A study by *Seyedali et al. (2021)* examined the effect of pH on the $\delta^7\text{Li}$ value and D_{Li} in inorganic calcite that recrystallized from vaterite in an experimental solution. They observed that increasing solution pH resulted in a decrease in D_{Li} but an increase in the $\delta^7\text{Li}$ values of calcite. *Füger et al. (2019)* quantified D_{Li} as a function of pH and growth rate in inorganic calcite, also observing a decrease in D_{Li} with increasing pH values. *Füger et al. (2021)* reported a decrease in the $\delta^7\text{Li}$ values of inorganic calcite samples with increasing growth rate and pH, noting that under similar precipitation rates (constant kinetic effects), there was actually a positive correlation between pH and the $\delta^7\text{Li}$ values of the calcite samples. *Day et al. (2021)* focused on the effect of temperature and growth rate on the $\delta^7\text{Li}$ values and D_{Li} in inorganic calcite, high-magnesian calcite, and aragonite precipitated from cave-analogue precipitation experiments. While they observed no significant effect on D_{Li} or $\delta^7\text{Li}$ value from temperature, they did suggest that other factors such as growth rate could impact Li incorporation. However, in many of these studies, individual solution parameters were not necessarily manipulated systematically (i.e., multiple parameters co-varied). This calls for additional and more systematic experiments to identify the potential controls on lithium isotopic and elemental incorporation into CaCO_3 minerals.

While previous studies provide some valuable insight, there are still gaps in the foundational knowledge of the controls on Li incorporation in carbonate minerals. This includes the potential effects of individual dissolved carbonate chemistry parameters varied in isolation, effects due to precipitation kinetics, and effects due to mineralogical differences in calcium carbonate phases. In order to confidently use the $\delta^7\text{Li}$ value and Li/Ca in biogenic CaCO_3 as proxies for silicate weathering, it is necessary to first establish foundational understanding on the individual physico-chemical controls on the $\delta^7\text{Li}$ value and Li/Ca in inorganic CaCO_3 through systematic precipitation experiments. To this end, the present study conducted multiple series of systematic inorganic precipitation experiments for both calcite and aragonite under identical conditions. Single-parameter manipulation experiments varied chemical parameters (pH, [DIC] and $[\text{Ca}^{2+}]$) from a baseline condition to observe the individual effects of these parameters on the $\delta^7\text{Li}$ values and Li/Ca of aragonite and calcite. Additionally, a combined parameter series

manipulated both $[Ca^{2+}]/pH$ to maintain a constant precipitation rate, which compared with the single-parameter manipulation series, will allow separation of effects due to carbonate chemistry from precipitation kinetics.

2. METHODS

2.1 Overview

Inorganic experiments conducted in the present study followed an approach adopted from *Sanyal et al. (2000)* and *Uchikawa et al. (2015)*, in which $CaCO_3$ precipitation occurred as overgrowth on the surface of seeds added to the experimental solutions. This “seeded” method has a few benefits over other “non-seeded” methods for the present application. Firstly, the parent solution is prepared to a saturation range where precipitation can be initiated only after seed addition. This allowed for precise identification of the timing at which precipitation began as well as minimized the potential of spontaneous $CaCO_3$ nucleation and precipitation. Secondly, the seeds serve as mineralogical templates for the overgrowth, such that calcite seeds induce calcite overgrowth and aragonite seeds induce aragonite overgrowth even when an experimental condition favors one or the other of the polymorphs (*Zeebe & Sanyal, 2002; Romanek et al., 1992; Mucci et al 1989*). And thirdly, such templated mineral growth is somewhat analogous to biomineralization by marine calcifiers (e.g., foraminifera), in which organic matrices are known to play significant role for the mineralogy and morphology of $CaCO_3$ secreted by organisms (*Zeebe & Sanyal, 2002; Erez, 2003; de Nooijer et al. 2014*).

Experiments were conducted using a pH-stat system (see **Figure 2**) and followed similar methods as described in *Uchikawa et al. (2015)*. The acrylic reaction chamber was sealed airtight and submerged in a water bath to maintain a temperature of 25 °C. The chamber was connected to a titration system via a pH electrode (Thermo Scientific #8104BNUWP), which was calibrated before each experiment using NIST pH buffers. The electrode sent voltage readings to the titrator system every second, averaging these signals over a 10 second interval to log the pH of the experimental solution. If the pH reading fell below the assigned value by 0.01 units, the system dosed 20 μ L of titrant (0.3 M NaOH or 0.3 M ^{13}C -spiked Na_2CO_3 solution - $\delta^{13}C = +150\text{‰}$ vs. VPDB) to the reactor through a gas-impermeable tube. The Na_2CO_3 solution used was ^{13}C -spiked to apply ^{13}C mass balance calculations for quantifying the overgrowth fraction in the $CaCO_3$ samples (detailed in Section 2.5).

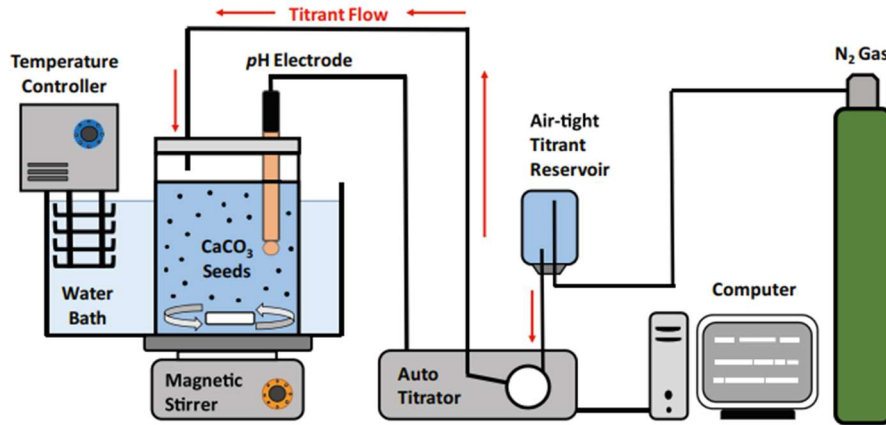
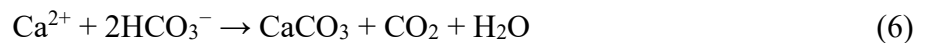


Figure 2: Experimental Set Up

Illustration of experimental set up (Uchikawa *et al.*, 2015). CaCO_3 seeds are added to the reactor, which is kept inside a temperature-controlled water bath. The pH electrode sends signals to the computer to track pH of experimental solution. As precipitation occurs and pH decreases, the auto titrator delivers 20 μL of ^{13}C -spiked Na_2CO_3 solution to reactor. N_2 gas delivered to titrant reservoir maintains consistent air pressure within the air-tight system.

The experimental solution was prepared before each experiment in a 1 L volumetric flask by adding CaCl_2 , MgCl_2 , LiCl , and a small amount of 1 N HCl solutions into ~ 800 mL of Milli-Q ultrapure deionized (DI) H_2O . This mixture in the flask was then kept in the water bath to come to 25 $^\circ\text{C}$. Subsequently, a 100 mL flask of ^{13}C -spiked Na_2CO_3 (the source of DIC) was added to the 1 L flask and the solution was brought up to a total of 1 L with additional DI water. The experimental solution prepared as described above was then transferred and sealed in the reactor chamber, which was placed in the water bath. This was followed by titration with 0.3 M NaOH to the desired pH and up to ~ 2 hours of chemical equilibration.

Following chemical equilibration, the titrant was switched to 0.3 M ^{13}C -spiked Na_2CO_3 , and 30 mg of either calcite or aragonite seeds were added to initiate precipitation. The reaction of CaCO_3 precipitation may be written as follows:



As CaCO_3 precipitates, there is a decrease in solution pH, DIC, and total alkalinity (Zeebe & Wolf-Gladrow, 2001). These changes were balanced by the addition 0.3 M ^{13}C -spiked Na_2CO_3 solution to maintain a relatively stable pH, alkalinity, and DIC concentration over the experimental duration. **Figure 3** shows a plot of the pH readings and titrant addition by the pH-

stat system during an experimental run. Note that the pace of titrant addition is indicative of the rate of CaCO_3 precipitation.

Experiments were usually terminated after sequential addition of $\sim 1500 \mu\text{L}$ of the Na_2CO_3 titrant, which typically resulted in precipitation of 25 to 30 mg of new CaCO_3 overgrowth and a final CaCO_3 sample consisting of approximately an equal mass proportion of the seeds and overgrowth. At the termination of each experiment, the solution was filtered using a vacuum filtration unit through a $0.2 \mu\text{m}$ cellulose-nitrate membrane filter and the CaCO_3 sample was rinsed with DI water and dried in an oven at approximately 60°C for at least 24 hours. A small volume of the experimental solution was also sampled prior to seed addition (pre-precipitation) and after filtration (post-precipitation).

2.2 Experimental Design

Chemical modifications were applied to the same baseline (control) solution prepared to the chemical composition of $[\text{Ca}^{2+}] = 5.25 \text{ mM}$, $[\text{Mg}^{2+}] = 3.5 \text{ mM}$, $[\text{Li}^+] = 0.25 \text{ mM}$, and $[\text{DIC}] = 2.1 \text{ mM}$. The baseline $[\text{DIC}]$ of 2.1 mM , is reasonably close to the average $[\text{DIC}]$ of modern

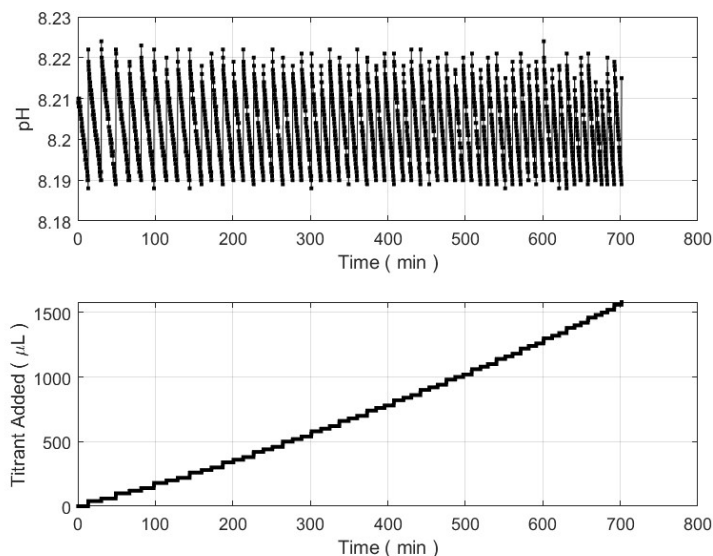


Figure 3: pH-Stat System Titration Plot

pH-stat system titration plot from a precipitation experiment displaying pH reading vs time in minutes (top) and titrant addition vs time (bottom). pH was relatively constant within a range of ~ 0.03 units. The addition of titrant is reflective of the rate of CaCO_3 precipitation.

seawater (2.39 mM). The $[Ca^{2+}]$ of the solution is half that of seawater in order to maintain a saturation low enough to prevent spontaneous precipitation of $CaCO_3$, but high enough to trigger $CaCO_3$ precipitation with the aid of adding seed minerals. The $[Li^+]$ of the experimental solution is ~10 times that of seawater (26 μM) (Misra & Froelich, 2012), to ensure that the $CaCO_3$ samples have high enough Li concentrations for δ^7Li measurements. The parent solution composition and Saturation Index (SI) for each experimental condition within each series is listed in **Table 1**. SI is defined by the following equation (Uchikawa et al., 2015):

$$SI = \frac{\log_{10}Q}{K_{sp}} \quad (7)$$

where Q refers to the ion activity product of Ca^{2+} and CO_3^{2-} and K_{sp} refers to the thermodynamic solubility product for calcite and aragonite ($K_{sp} = 10^{-8.48}$ and $10^{-8.34}$ for calcite and aragonite, respectively, at 25 °C: Plummer & Busenberg, 1982). The SI for calcite ($SI_{Calcite}$) and aragonite ($SI_{Aragonite}$) under various experimental solution conditions was constrained using the PHREEQC aqueous geochemical model (Parkhurst & Appelo, 1999) in conjunction with WATEQF thermodynamic database (Ball & Nordstrom, 1991), as described in Uchikawa et al. (2015).

When $CaCO_3$ precipitates from aqueous solutions spontaneously in the absence of any seeds, the mineralogy of the resulting $CaCO_3$ strongly depends on the $[Mg^{2+}]$ and temperature of the solutions (Wray & Daniels, 1957; Morse & Wang 1997). To enable selective precipitation of either aragonite or calcite, the “seeded” method was used to provide a nucleation site and promote the precipitation of homogeneous overgrowth (Zeebe & Sanyal, 2002; Romanek et al., 1992; Mucci et al 1989).

Nonetheless, trial experiments conducted at 25 °C using aragonite seeds always resulted in overgrowth consisting of a mixture of calcite and aragonite when the experimental solution consisted of a $[Mg^{2+}]:[Ca^{2+}]$ ratio of 1:4 (see Section 3.2). Experiments using calcite seeds consistently resulted in low-Mg calcite overgrowth. After testing a variety of $[Mg^{2+}]:[Ca^{2+}]$ ratios in multiple trial experiments, a $[Mg^{2+}]:[Ca^{2+}]$ ratio of 1:1.5 was found to be optimal for calcite and aragonite precipitation under identical conditions.

Table 1: Summary of Chemical Manipulations and Experimental Solution Composition

		Solution Chemistry						
Parameter		[Ca ²⁺]	[Mg ²⁺]	[Li ⁺]	[DIC]	pH	Saturation	
Series	Manipulations	mM	mM	mM	mM		index	
Control		5.25	3.5	0.25	2.1	8.2	SI _{Calcite} = 1.02 SI _{Aragonite} = 0.87	
pH	pH=8.0	5.25	3.5	0.25	2.1	8	SI _{Calcite} = 0.82 SI _{Aragonite} = 0.68	
	pH=8.4	5.25	3.5	0.25	2.1	8.4	SI _{Calcite} = 1.20 SI _{Aragonite} = 1.06	
[DIC]	1.5x[DIC]	5.25	3.5	0.25	3.15	8.2	SI _{Calcite} = 1.19 SI _{Aragonite} = 1.04	
	0.75x[DIC]	5.25	3.5	0.25	1.575	8.2	SI _{Calcite} = 0.89 SI _{Aragonite} = 0.75	
[Ca ²⁺]	1.5x[Ca ²⁺]	7.875	5.25	0.25	2.1	8.2	SI _{Calcite} = 1.16 SI _{Aragonite} = 1.01	
	0.5x[Ca ²⁺]	2.625	1.75	0.25	2.1	8.2	SI _{Calcite} = 0.75 SI _{Aragonite} = 0.61	
[Ca ²⁺]/pH	1.5x[Ca ²⁺]/pH=8	7.875	5.25	0.25	2.1	8	SI _{Calcite} = 0.95 SI _{Aragonite} = 0.80	
	0.5x[Ca ²⁺]/pH=8.4	2.625	1.75	0.25	2.1	8.4	SI _{Calcite} = 0.94 SI _{Aragonite} = 0.80	

Single parameter manipulation series (pH, [DIC], and $[\text{Ca}^{2+}]$) consisted of a baseline condition and a high and low end-member. Each experimental condition was repeated for both calcite and aragonite under identical chemical conditions. Additionally, a combined-parameter series varied pH and $[\text{Ca}^{2+}]$ at a fixed saturation (matched with the baseline conditions) so that the rate of precipitation was relatively constant.

While the pH-stat system was capable of maintaining constant DIC, alkalinity, and pH over the course of the experiment via the titrated addition of 0.3 M Na_2CO_3 , it did not have the capability to compensate for Ca^{2+} drawdown. The addition of $\sim 1500 \mu\text{L}$ of Na_2CO_3 over the experiment duration also inevitably resulted in a buildup of Na^+ in the experimental solution (detailed in Results).

2.3 Preparation of Stock Solutions

As described in Section 2.1, experimental solutions were prepared by mixing a set of stock solutions. The CaCl_2 stock solution was prepared to a concentration of about 1 M by dissolving $\text{CaCl}_2 \cdot 2\text{H}_2\text{O}$ into 1 L of deionized water due to the hygroscopic nature of the salt (hence the difficulty in accurately weighing the salt on a high-precision balance). Precise concentration of the stock solution was determined later based on Mohr titration to measure $[\text{Cl}^-]$ (Yoder, 1919). The same steps were taken to prepare the MgCl_2 and LiCl stock solution (note that $\text{MgCl}_2 \cdot 6\text{H}_2\text{O}$ salt was used for the former).

The stock Na_2CO_3 solution was ^{13}C -spiked ($\delta^{13}\text{C} = +150\text{‰}$ vs. VPDB), so that the newly precipitated CaCO_3 overgrowth would inherit the ^{13}C -enriched signature (further detailed in Section 2.5). To avoid absorption of atmospheric CO_2 , both Na_2CO_3 and NaOH solutions were prepared in a glove-bag under an N_2 atmosphere. The DI water used for the experimental solution, Na_2CO_3 , and NaOH preparation was bubbled with N_2 gas to ensure solutions were free of CO_2 . Additionally, during the preparation of the experimental solution in the 1 L volumetric flask, the flask was also purged with N_2 gas to minimize CO_2 absorption.

The Na_2CO_3 stock solutions were prepared in a glove-bag under an N_2 atmosphere by dissolving a mixture of non-labeled and ^{13}C -labeled Na_2CO_3 (in amounts to yield 0.3 M Na_2CO_3 with a $\delta^{13}\text{C}$ value of $+150\text{‰}$) in 1 L of N_2 bubbled DI water. The mixture was stirred for ~ 60 minutes to ensure total dissolution of Na_2CO_3 . Aliquots of the Na_2CO_3 solution were reacted with BaCl_2 to quantitatively form BaCO_3 solids as a record of the ^{13}C -spike (e.g., Uchikawa &

Zeebe, 2012). The $\delta^{13}\text{C}$ values of these BaCO_3 samples (**Table A1**, see Appendix) were analyzed and used to constrain the $\delta^{13}\text{C}$ value of the calcite and aragonite overgrowth precipitated during the experiments, as needed for the mass balance calculations to quantify the overgrowth fraction in the samples (see Section 2.5 for more details). Following removal from the N_2 atmosphere environment, BaCO_3 samples were immediately vacuum filtered onto a $0.2\ \mu\text{m}$ cellulose-nitrate membrane filter and dried. In separate 100 mL volumetric flasks, $0.3\ \text{M}$ ^{13}C -labeled Na_2CO_3 was diluted with N_2 bubbled DI water to the desired [DIC] to be used in the experimental solution. The flasks also contained a small amount of $1\ \text{N}$ HCl for pH adjustment. The $0.3\ \text{M}$ NaOH solution was also prepared in a glove-bag under an N_2 atmosphere by dissolving NaOH salt in 1 L of water and stirred for ~ 60 minutes to ensure complete dissolution. The NaOH and remaining Na_2CO_3 solutions were sealed in 15 mL high density polyethylene (HDPE) bottles to be used as titrants for CaCO_3 precipitation experiments. Both the HDPE bottles and 100 mL flasks were stored in desiccators which were vacuumed and re-filled with N_2 gas.

2.4 Preparation and Characterization of CaCO_3 Seeds

The calcite seeds used for the present experiments were from the same batch previously used in *Uchikawa et al. (2015; 2017)* that was originally purchased from Sigma-Aldrich. The seeds were used as is, without any further treatment or cleaning. The aragonite seeds were prepared in the laboratory using a method modified from *Mavromatis et al. (2018)* in which 40 mL of $1.25\ \text{M}$ Na_2CO_3 was added dropwise at a rate of roughly $2.5\ \text{mL/s}$ into a 750 mL of solution prepared to $0.1\ \text{M}$ CaCl_2 , $0.1\ \text{M}$ MgCl_2 , and $0.4\ \text{M}$ NaCl at $80 \pm 2\ ^\circ\text{C}$ while constantly stirred at approximately 250 rpm. Upon dropwise addition of the Na_2CO_3 solution to the other reactive solution, precipitation of CaCO_3 began immediately. Once all of the Na_2CO_3 solution was added, the precipitates were separated from the solution mixture and collected onto a $0.2\ \mu\text{m}$ cellulose-nitrate membrane filter by vacuum filtration. Immediately after the collection, the precipitates were rinsed rigorously with ultra-pure deionized water and dried at $60\ ^\circ\text{C}$ for at least 24 hours. The seeds were then analyzed both with Raman spectroscopy and XRD to confirm the mineralogy of the resultant precipitates as pure aragonite.

Both calcite and aragonite seeds were isotopically homogeneous and essentially free of Li (**Table 2**) so that the total Li in the CaCO_3 sample (= seeds + overgrowth) was exclusively derived from the overgrowth fraction. The surface area of calcite and aragonite seeds were

measured using the Brunauer-Emmett-Teller (BET) method (*Brunauer et al., 1938*). BET measurements were conducted on ~1g of the calcite and aragonite seeds by a Quantachrome instrument Autosorb IQ machine using nitrogen and 25 measured adsorption points.

Approximately ~1 g of seed sample was analyzed.

Table 2: Calcite and Aragonite Seed Characteristics
Including $\delta^{13}\text{C}$ and $\delta^{18}\text{O}$ values, Li/Ca ratio values, and average surface area from BET measurements.

	$\delta^{13}\text{C}$ (VPDB)		$\delta^{18}\text{O}$ (VPDB)		Li/Ca	Surface Area
	‰		‰		$\mu\text{mol/mol}$	m^2/g
Calcite	-17.89	± 0.005	-21.24	± 0.009	2.41	0.22
Aragonite	-2.627	± 0.003	-15.93	± 0.009	0.35	1.24

2.5 ^{13}C Mass Balance

Mass balance calculations were used to determine the mass and Li/Ca ratios of overgrowth for each sample following methods described in *Uchikawa et al. (2015)* and the following equations:

$$\delta^{13}\text{C}_{\text{Sample}} = (f_{\text{OG}}) \times (\delta^{13}\text{C}_{\text{OG}}) + (1 - f_{\text{OG}}) \times (\delta^{13}\text{C}_{\text{Seeds}}) \quad (8)$$

$$(\text{Li/Ca})_{\text{Sample}} = (f_{\text{OG}}) \times ((\text{Li/Ca})_{\text{OG}}) + (1 - f_{\text{OG}}) \times ((\text{Li/Ca})_{\text{Seeds}}) \quad (9)$$

where the mass-fraction of overgrowth relative to the total sample mass (f_{OG}) was calculated by equation (8) with the inputs of the measured $\delta^{13}\text{C}$ values of the total sample ($\delta^{13}\text{C}_{\text{Sample}}$) and the seeds ($\delta^{13}\text{C}_{\text{Seeds}}$), along with the expected $\delta^{13}\text{C}$ values of the CaCO_3 overgrowth that were determined from the extent of ^{13}C -spike applied to the Na_2CO_3 solutions (reflected by the BaCO_3 samples: see Section 2.3). The BaCO_3 samples quantitatively precipitated from the ^{13}C -spiked Na_2CO_3 solutions specifically reflected the $\delta^{13}\text{C}$ value of solution CO_3^{2-} (**Table A1**, see Appendix). Given the experimental pH range of 8.0 to 8.4, bicarbonate (HCO_3^-) was the dominant DIC species in the experimental solution. By applying the fractionation between CO_3^{2-} and HCO_3^- , ($\epsilon_{\text{carbonate-bicarbonate}} = -1.992\text{‰}$, determined using equations from *Zhang et al., 1995*), the $\delta^{13}\text{C}$ value of solution HCO_3^- can be estimated using Equation (4).

The fractionation factor between calcite or aragonite and HCO_3^- ($\epsilon_{\text{Calcite-bicarbonate}} = 1.0\text{‰}$ and $\epsilon_{\text{Aragonite-bicarbonate}} = 2.7\text{‰}$) established by *Romanek et al. (1992)* was used to calculate the $\delta^{13}\text{C}_{\text{OG}}$ value. The $\delta^{13}\text{C}_{\text{OG}}$ value was then used in equation (9) with the measured $(\text{Li/Ca})_{\text{sample}}$

and $(\text{Li}/\text{Ca})_{\text{Seeds}}$ values (**Table 2**) to find the Li/Ca ratio in the overgrowth fraction, $(\text{Li}/\text{Ca})_{\text{OG}}$. This method allows for a more accurate measurement of the Li/Ca ratio in the overgrowth sample yield even in the event of spills or sample-loss during post-precipitation sample collection.

Since carbonate speciation is pH dependent, the $\delta^{13}\text{C}$ value of each individual DIC species (i.e., CO_2 , HCO_3^- , and CO_3^{2-}) within a total DIC pool of a known $\delta^{13}\text{C}$ value can vary as a function of pH (*Zeebe & Wolf-Gladrow, 2001*). Given the pH range tested in the present study (8.0 to 8.4), the $\delta^{13}\text{C}$ value for HCO_3^- in the experimental solution would vary by no more than about 1‰. This uncertainty assigned to the $\delta^{13}\text{C}_{\text{OG}}$ estimates is fairly insignificant in the error propagation, which was determined following methods described in *Fitzsimon et al. (2000)*. Given the mass-balance equations, even if the fractionation between HCO_3^- and CaCO_3 solids had an uncertainty as high as 3‰, the uncertainty in $(\text{Li}/\text{Ca})_{\text{OG}}$ values would be constrained within ~1% error (for more details see: *Uchikawa et al., 2015*).

2.6 Analytical Methods

2.6.1 $\delta^{13}\text{C}$ Analysis

All of carbonate materials and samples (i.e., calcite and aragonite seeds, BaCO_3 samples prepared upon preparation of the ^{13}C -labeled Na_2CO_3 solutions, and CaCO_3 samples from the precipitation experiments) were sent to the University of California Santa Cruz (UCSC) Stable Isotope Laboratory for $\delta^{13}\text{C}$ analysis, as detailed in *Uchikawa et al (2015)*. Briefly, samples were reacted with orthophosphoric acid at 77 °C and then analyzed on a ThermoFinnegan 253 dual-inlet isotope radio mass spectrometer coupled with a Kiel IV carbonate device. Duplicate measurements were averaged to determine sample $\delta^{13}\text{C}$ value (standardize to reference material VPDB), with an average sample reproducibility of $\pm 0.15\text{‰}$.

2.6.2 Elemental Analysis

Li/Ca, Na/Ca, and Mg/Ca analyses were conducted by this author at the Centre for Earth Sciences at the Indian Institute of Science. Sample preparation prior to analysis followed methods described in *Misra et al. (2014)*. Calcite and aragonite samples were aliquoted into pre-cleaned 0.5 mL micro-centrifuge tubes and leached by adding approximately 0.3 mL of 0.001 N HNO_3 to remove any potential surface adsorbed elements in the samples. The samples and acid

were thoroughly mixed using a vortex mixer. After the sample and acid mixtures were centrifuged, the supernatant in each microcentrifuge tube was pipetted off and discarded. This procedure was repeated twice before finally dissolving the CaCO₃ samples by adding 150 µl of 1N HNO₃. The HCl and HNO₃ acids used in these processes were double-distilled and diluted using 18.2 MOhm MilliQ water.

A 20 µL aliquot of the dissolved sample was added to 270 µL of 2% HNO₃ to prepare for analysis. The calcium concentration was determined using matrix matched calibration standards by the inductively coupled plasma optical emission spectroscopy (Agilent 5800 ICP-OES). These concentrations were then used to dilute samples to a constant calcium concentration of ~60 ppm. Samples were analyzed for Li/Ca by a triple quadrupole ICP-MS (Agilent 8900 QQQ-ICP-MS) against external calibration standards of fixed [Ca²⁺] (60 ppm) and variable [Li⁺]. All samples were analyzed in groups of 14 bracketed by acid blanks and standards to correct for instrumental background and drift.

2.6.3 δ⁷Li Analysis

Separation and purification of Li from the samples for δ⁷Li analysis was done by this author, and followed a method adapted from *Bohlin et al. (2018)*. 1.5 mL of AGMP-50 cation exchange resin was loaded onto individual columns with the height and inner diameter of 20 cm and 3 mm, respectively. The resin was rinsed twice with 10 N HCl and MilliQ water prior to sample elution, and then resuspended by backwashing, allowing it to settle and create a homogeneous bed of resin inside the column. The resin was conditioned with 5 mL of 0.5 N HCl and dissolved CaCO₃ samples were loaded in quantities containing 1-2 ng of Li. Columns were then washed with 6 mL of 0.5 N HCl before Li was eluted in a 6 ml cut, which was collected in acid cleaned Savillex Teflon vials. A 1 mL cut was collected before and after Li elution to ensure 100% yield within the Li cut (*i.e.*, both the first and last 1 mL cut was virtually Li-free). After collection, samples were dried down on a hotplate at 110 °C and then redissolved in 200 µL of 2% HNO₃.

Lithium isotope ratios were measured by a single collector triple quadrupole ICP-MS (Agilent 8900 QQQ-ICP-MS) at the Indian Institute of Science following methods described in *Juzer et al. (2022)*. Measurements were performed under cool plasma conditions (forward RF power of 600 W) and used a sample introduction system with an 80 µL/min self-aspirating

nebulizer and 2.5 mm demountable quartz torch with a sapphire injector. Samples were measured in duplicate and bracketed by NIST SRM 8545 (LSVEC) standards and acid blanks to account for instrument drift. Mismatched ion counts between the sample and the standards can impact the measured sample $\delta^7\text{Li}$ values. To avoid this, a 20 μL aliquot of each sample was diluted with 480 μL of 2% HNO_3 and measured relative to the bracketing standard. The ion counts were compared, and samples diluted so that the ^7Li counts matched those of the bracketing standard (10^6 cps).

3. RESULTS

3.1 Visual and Mineralogical Characterization of CaCO_3 Seeds

Scanning Electron Microscopy (SEM) imaging of aragonite and calcite seeds were conducted at the Centre for Earth Sciences at the Indian Institute of Science in Bangalore. Aragonite seeds (**Figure 4A**) were hexagonal prismatic crystals with a length of approximately 10 μm . Calcite seeds (**Figure 4C**) were rhombohedral in shape and approximately 10 μm in size. Aragonite seeds were analyzed at the University of Hawai'i using Raman Spectroscopy to determine their mineralogy. The signal peaks (**Figure A1**, see Appendix) from the aragonite seed analysis matched those described for aragonitic CaCO_3 in *De La Pierre et al. (2014)*.

Figure 4 also compares the SEM images of calcite and aragonite seeds (**4A & 4C**) before and after the precipitation experiments (**4B & 4D**). The aragonite crystals appeared to have grown fairly uniformly, maintaining their hexagonal crystal structure. The calcite, however, did not precipitate over the surfaces evenly, resulting in a distorted structure with uneven surfaces.

3.2 Trial Experiments

Despite the use of calcite and aragonite seeds in the present study to control and dictate the mineralogy of the new CaCO_3 overgrowth (e.g., *Zeebe & Sanyal, 2002; Romanek et al., 1992; Mucci et al., 1989*; See Section 2.2), one unsettled concern was that solution chemical composition (namely, the solution $[\text{Mg}^{2+}]:[\text{Ca}^{2+}]$ ratio: *Wray & Daniels, 1957; Morse & Wang, 1997*) would also have an impact on the sample mineralogy. Thus, before starting the planned experiments (**Table 1**), trial runs were conducted to determine the optimum solution chemistry to successfully achieve pure calcite and aragonite precipitation under the same experimental conditions. It was important that experimental runs using aragonite seeds resulted in pure

aragonite samples (and correspondingly for calcite) to minimize any experimental bias on Li incorporation resulting from mixed mineralogy.

The CaCO_3 samples produced from these trial experiments were analyzed using Raman Spectroscopy and/or X-Ray Diffraction (XRD) to determine the mineralogy of the overgrowth. Initially, a simple experimental solution consisting of CaCl_2 , LiCl , ^{13}C -spiked Na_2CO_3 , and no Mg^{2+} was tested for the resulting CaCO_3 mineralogy. From this Mg-free solution, the CaCO_3 overgrowth precipitated over calcite seeds showed Raman signal peaks indicative of calcite. However, the precipitate formed over aragonite seeds produced signals with peaks indicative of both calcite and aragonite. These results are in line with the notion that Mg-free solutions at a temperature of $25\text{ }^\circ\text{C}$ promote calcite precipitation instead of aragonite precipitation (*Morse & Wang, 1997*).

Given the results described above, additional trial experiments were conducted under two different solutions [Mg^{2+}]:[Ca^{2+}] ratios (1:4 and 1:1.5), and the resultant CaCO_3 samples were analyzed using XRD. At the ratio of 1:4, samples produced from the test runs with aragonite

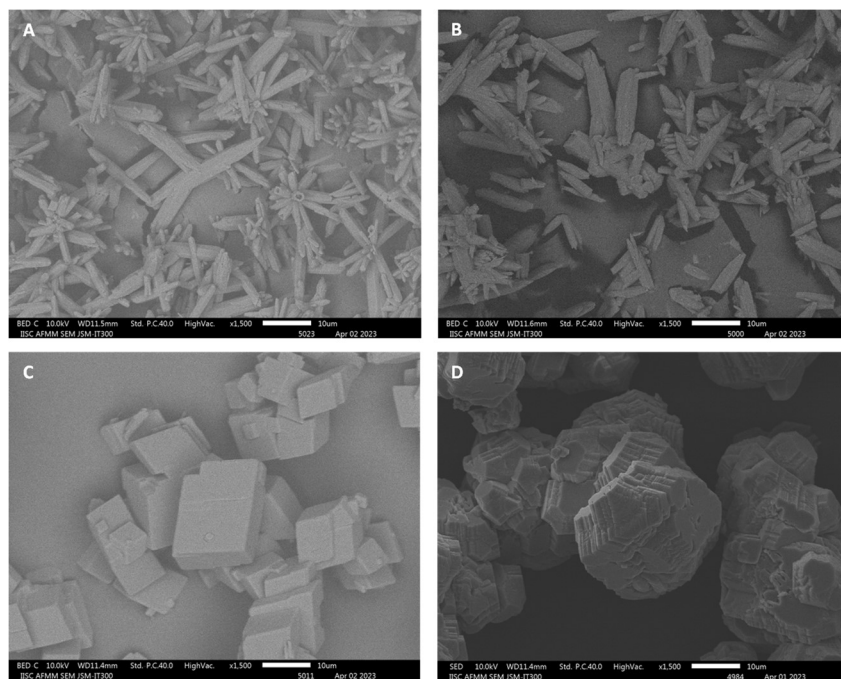


Figure 4: SEM Images of CaCO_3 Samples

(A) aragonite seeds, (B) aragonite crystals with overgrowth collected after a control experiment, (C) calcite seeds, and (D) calcite crystals with overgrowth collected after a control experiment.

seeds consisted of 70% aragonite and 30% calcite. At the ratio of 1:1.5, samples produced from the test runs with aragonite seeds represented 91.2% aragonite and 8.8% calcite, whereas those prepared with calcite seeds were 100% calcite. To ensure overgrowth on aragonite seeds was at least 90% aragonite, the $[\text{Mg}^{2+}]:[\text{Ca}^{2+}]$ ratio used in the experimental solution was set at 1:1.5 even when solution $[\text{Ca}^{2+}]$ was varied.

3.3 Experimental Solution and Parameter Manipulations

Experimental solutions sampled prior to seed addition (pre-precipitation) and following sample filtration (post-precipitation) were analyzed for elemental composition on the ICP-OES to a precision of $\pm 2\%$ (2σ) and are summarized in **Table A4** (See Appendix). It was estimated that, in order to produce ~25 to 30 mg of new CaCO_3 overgrowth at the baseline condition ($[\text{Ca}^{2+}] = 5.25 \text{ mM}$), solution $[\text{Ca}^{2+}]$ would decrease by 5 to 10% over the duration of the experiment. Indeed, the results from ICP-OES analyses of experimental solution samples indicated an approximately 5 to 10% decrease in solution $[\text{Ca}^{2+}]$ before and after the CaCO_3 precipitation experiments performed at the initial concentration of 5.25 mM. Experiments conducted at a lower initial $[\text{Ca}^{2+}]$ of 2.625 mM experienced a greater decrease (10 to 15%) in $[\text{Ca}^{2+}]$ over the duration of the experiment. However, this decrease did not slow down the overall pace of titrant addition during the length of an experiment, indicating that the precipitation rate was not affected by Ca^{2+} drawdown, possibly balanced by an increase in surface area as overgrowth precipitated over the seeds.

As Na_2CO_3 was the source of DIC in the experimental parent solution, the starting $[\text{Na}^+]$ of the experimental solution varied depending on the [DIC]. Experimental runs conducted at a baseline [DIC] of 2.1 mM had an initial $[\text{Na}^+]$ of approximately 5 mM. The [DIC] series experiments performed at [DIC] = 1.575 mM had a lower initial $[\text{Na}^+]$ of approximately 3.5 mM, whereas experiments run at [DIC] = 3.15 mM had a higher initial $[\text{Na}^+]$ of approximately 7 mM. The addition of ~1500 μl of Na_2CO_3 titrant over the duration of the experiment resulted in a buildup of Na^+ by a concentration of approximately 1 mM. During some calcite and aragonite experimental runs (24 out of 46 runs in total), there was a slight increase (less than 1 mM) in $[\text{Mg}^{2+}]$ in the post-precipitation solution, possibly due to impurities of Mg^{2+} in the Na_2CO_3 salt used during the preparation of the Na_2CO_3 stock solutions.

The average precipitation rate (R) of calcite and aragonite samples were determined by using the quantity of overgrowth (from f_{OG}), experimental run time, and seed surface area. Surface area was calculated using BET measured average surface area values and the mass of the respective seeds added (30 mg). Due to the small experimental sample yield (less than 1 g), it was not possible to reliably analyze samples for post-precipitation surface area measurements. Additionally, variation in aragonite seed size and the lack of uniformity in calcite overgrowth made it difficult to constrain the change in surface area confidently. Thus, only initial surface area values were used in rate estimations.

R is reported in unit of mol/m²/s and ranged from 10^{-6.5} to 10^{-5.4} mol/m²/s for calcite and 10^{-6.9} to 10^{-6.0} mol/m²/s for aragonite (**Table A3**, see Appendix). During each single-parameter series, there was an increase in R with an increase in pH, [DIC], and [Ca²⁺]. This is due to the saturation increasing under higher solution pH, [DIC], and [Ca²⁺]. During the combined [Ca²⁺]/pH parameter series, the parent solutions had a similar saturation, resulting in a similar average precipitation rate across all experiments.

3.4 Elemental and Isotopic Composition of Samples

The average $\delta^{13}\text{C}$ value were determined from duplicate measurements, with an average sample reproducibility of $\pm 0.15\text{‰}$ (1σ , $n = 13$). This is similar to the reproducibility reported for carbonate standards ($1\sigma = \sim \pm 0.1\text{‰}$). The approximate overgrowth mass for each sample was calculated from the mass-fraction of overgrowth (f_{OG}) determined using the ¹³C mass balance equations described in Section 2.5. Error was propagated using methods described in *Fitzsimons et al. (2000)*. The average overgrowth yield of CaCO₃ samples was 0.034 g (average $f_{OG} = 0.523 \pm 0.007$).

Li/Ca ratios for solids were measured on the QQQ-ICP-MS to a precision of $\pm 0.03\%$ (2σ) based on a standard reference material. Li/Ca ratios have been converted to D_{Li} values using Equation (3) and the measured Li/Ca ratios for solid and post-precipitation parent solution samples (**Table A4**, see Appendix). The $\delta^7\text{Li}$ values of samples are listed in **Table A3** (see Appendix), with a typical precision between ± 0.8 and $\pm 1.4\text{‰}$ (2σ , $n = 5$) based on an additional reference material (Li6-N-SRM) measured during each analytical session. The Li isotope fractionation factor between the solid CaCO₃ and experimental parent solution was determined

using Equation (3), the sample $\delta^7\text{Li}$ value, and the average solution pre-precipitation $\delta^7\text{Li}$ value of $+14.33 \pm 1.19\text{‰}$ ($n = 15, 1\sigma$) and is listed in **Table A3** (see Appendix). The average ${}^7\epsilon_{\text{solid-solution}}$ values are approximately $-3 \pm 1.0\text{‰}$ and $-16 \pm 1.3\text{‰}$ for all calcite and aragonite samples combined, respectively. Linear relationships in the data were analyzed using the Fit Linear Regression Model tool in MATLAB, which defines the R^2 and p-value for each set of data (**Table 3**).

Figure 5 shows the ${}^7\epsilon_{\text{solid-solution}}$ and D_{Li} values for calcite (filled symbols) and aragonite (open symbols) samples from each of the single-parameter series (pH, [DIC], and $[\text{Ca}^{2+}]$ were varied solely, while keeping other experimental conditions unchanged). There is a significant negative relationship between calcite ${}^7\epsilon_{\text{solid-solution}}$ values with changes in pH, but not with changes in [DIC] or $[\text{Ca}^{2+}]$. There is a significant positive correlation between Aragonite ${}^7\epsilon_{\text{solid-solution}}$ values with both [DIC] and $[\text{Ca}^{2+}]$. Aragonite ${}^7\epsilon_{\text{solid-solution}}$ also show a negative relationship with pH (however it is weaker and only significant at a 90% confidence level). There is

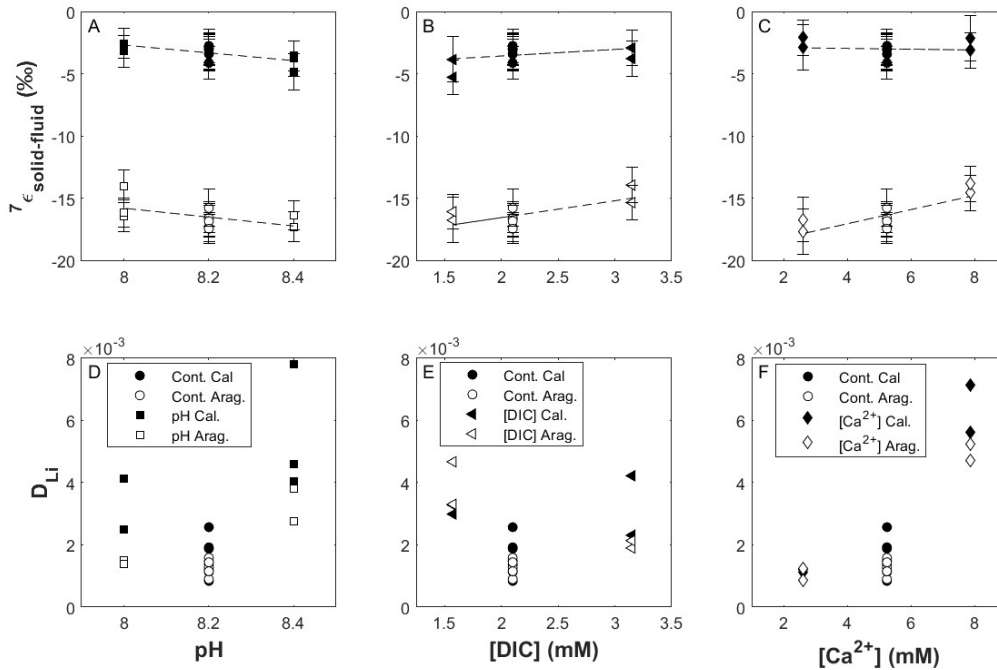


Figure 5: ${}^7\epsilon_{\text{solid-solution}}$ and D_{Li} Values from Individual Parameter Manipulation Experiments
 ${}^7\epsilon_{\text{solid-solution}}$ values for calcite (filled symbols) and aragonite (unfilled symbols) with variations in pH (A), [DIC] (B), $[\text{Ca}^{2+}]$ (C) as well as D_{Li} values for calcite (filled symbols) and aragonite (unfilled symbols) with variations in pH (D), [DIC] (E), and $[\text{Ca}^{2+}]$ (F). The abbreviation “Cont.” in legends refers to “Control” experiments.

consistently a large offset in $\delta^7\text{Li}$ values (~13% difference) between calcite and aragonite samples.

There is no statistically significant trend between D_{Li} and pH or [DIC] for either calcite or aragonite. However, there is an overall increase in both calcite and aragonite D_{Li} values from the low end-member (pH = 8.0, [DIC] = 1.575 mM) to the high end-member experiments (pH = 8.4, [DIC] = 3.15 mM) for the pH and [DIC] series. There is also a strong positive correlation between the D_{Li} values for both calcite and aragonite and solution $[\text{Ca}^{2+}]$.

The ${}^7\epsilon_{\text{solid-solution}}$ and D_{Li} values of the aragonite and calcite samples for the $[\text{Ca}^{2+}]/\text{pH}$ combined parameter series are shown in **Figure 6**. While there is no significant relationship between aragonite ${}^7\epsilon_{\text{solid-solution}}$ values and either $[\text{Ca}^{2+}]$ or pH, there is a positive correlation between calcite ${}^7\epsilon_{\text{solid-solution}}$ values and pH and negative correlation with $[\text{Ca}^{2+}]$. While there is no significant relationship between D_{Li} values for aragonite samples and $[\text{Ca}^{2+}]$ or pH, there is a significant trend with the calcite D_{Li} values, positively correlated with $[\text{Ca}^{2+}]$ and negatively correlated with pH.

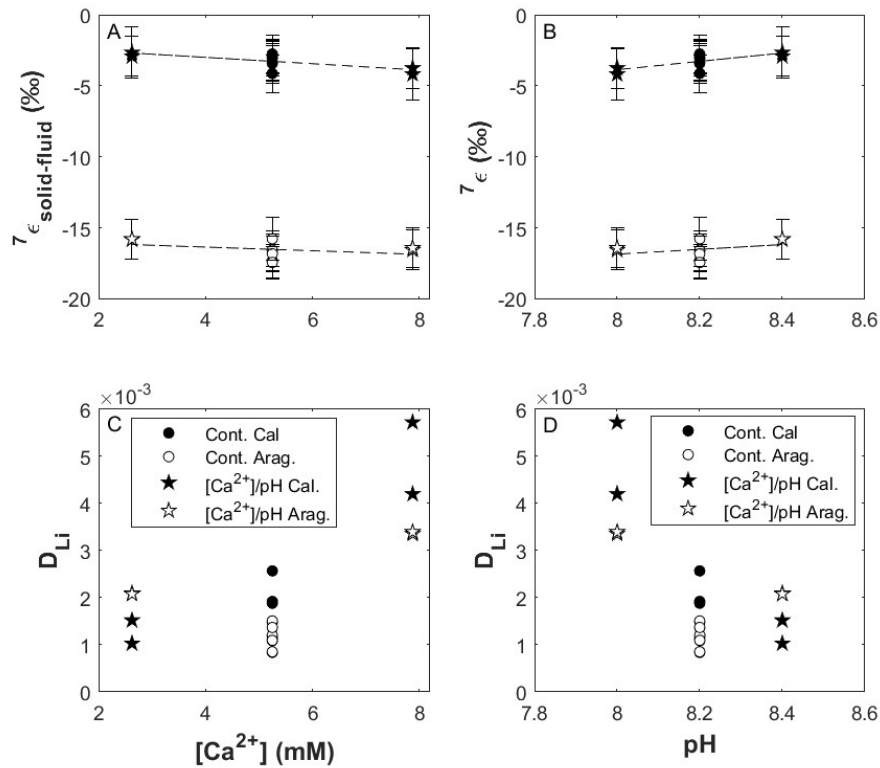


Figure 6: ${}^7\epsilon_{\text{solid-solution}}$ and D_{Li} Values from $[\text{Ca}^{2+}]/\text{pH}$ Manipulation Experiments Showing ${}^7\epsilon_{\text{solid-solution}}$ and D_{Li} values for calcite (filled symbols) and aragonite (unfilled symbols) with variations in $[\text{Ca}^{2+}]$ and pH.

Table 3: Statistical Analysis

R^2 values, p-values, and linear relationship calculated from Linear Regression from each parameter series for relationship between ${}^7\epsilon_{\text{solid-fluid}}$ and D_{Li} values of calcite and aragonite samples with changing parameter (pH, [DIC], $[\text{Ca}^{2+}]$, $[\text{Ca}^{2+}]/\text{pH}$, and $\text{Log}_{10}R$).

Parameter Series	Mineralogy	${}^7\epsilon_{\text{solid-fluid}}$			D_{Li}		
		R^2 value	p-value	Relationship	R^2 value	p-value	Relationship
pH	Calcite	0.417	0.017	$-3.12x + 22.25$	0.093	0.175	$0.0093x - 0.074$
	Aragonite	0.276	0.097	$-3.57x + 12.73$	0.191	0.115	$-0.002x + 0.019$
[DIC]	Calcite	0.133	0.243	$0.52x - 4.62$	0.061	0.437	$0.0005x + 0.980$
	Aragonite	0.488	0.024	$1.35x - 19.25$	0.115	0.337	$-0.0008x + 0.004$
$[\text{Ca}^{2+}]$	Calcite	0.008	0.776	$-0.32x - 2.83$	0.586	0.002	$0.0010x - 0.003$
	Aragonite	0.624	0.007	$0.57x - 19.32$	0.601	0.005	$0.0007x - 0.002$
$[\text{Ca}^{2+}]/\text{pH}$	Calcite	0.484	0.012	$-0.223x - 2.10$	0.534	0.004	$0.0007x - 0.002$
	Aragonite	0.142	0.283	$-0.13x - 15.84$	0.12	0.174	$0.0003x + 0.0005$
$\text{Log}_{10}R$	Calcite	0.048	0.291	$-0.58x - 6.67$	0.206	0.013	$0.003x + 0.230$
	Aragonite	0.076	0.202	$0.99x - 9.65$	0.199	0.033	$0.002x + 0.015$

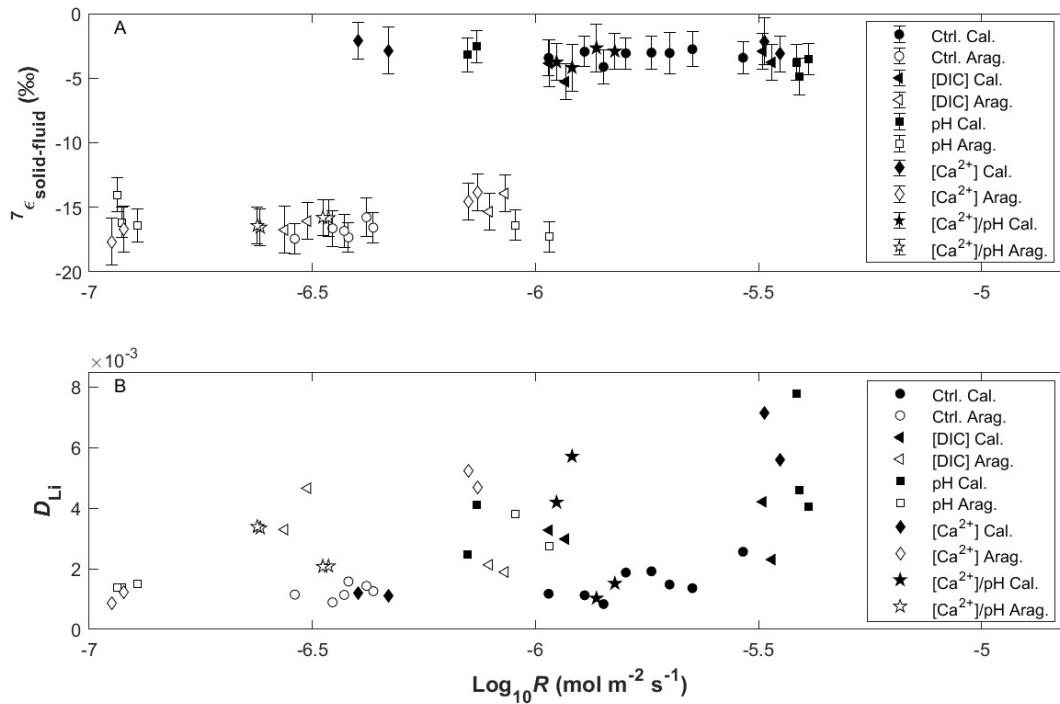


Figure 7: Relationship Between $\text{Log}R$ and ${}^7\epsilon_{\text{solid-solution}}$ and D_{Li} values

Log_{10} estimated rate of CaCO_3 precipitation (mol $\text{CaCO}_3/\text{m}^2/\text{s}$) for calcite (filled symbols) and aragonite (unfilled symbols) compared with ${}^7\epsilon_{\text{solid-solution}}$ values (A) and $\text{Log}_{10}D_{\text{Li}}$ values (B) for all experimental runs.

Figure 7 displays the relationship between $\text{Log}_{10}R$ and the ${}^7\epsilon_{\text{solid-solution}}$ and D_{Li} values for calcite and aragonite. There is no significant relationship between the rate of precipitation and the ${}^7\epsilon_{\text{solid-solution}}$ values for either calcite or aragonite. However, there is a weak positive trend between the $\text{Log}_{10}R$ and the D_{Li} values for both calcite and aragonite (see **Table 3**). It is important to note that while certain parameters may show a statistically significant relationship between the ${}^7\epsilon_{\text{solid-solution}}$ value of calcite or aragonite with changes in solution chemistry, the relationship is weak across all experimental series. Additionally, the relationship between the chemical parameters and ${}^7\epsilon_{\text{solid-solution}}$ values modeled by the linear regression (**Table 3**) result in a change in isotope fractionation of less than 2‰ for calcite samples and less than 3‰ for aragonite samples modeled across the range of parameters tested. This suggests changes in solution chemistry have minimal fractionation effects on calcite and aragonite within the range of chemical parameters tested, especially considering that the uncertainty for ${}^7\epsilon_{\text{solid-solution}}$ values is over 1‰.

4. DISCUSSION

4.1 Li Isotope Fractionation in Inorganic Calcite vs Aragonite

Both calcite and aragonite samples have lower $\delta^7\text{Li}$ values relative to the parent solution (negative ${}^7\epsilon_{\text{solid-solution}}$ values) indicating preferential uptake of ${}^6\text{Li}$ over heavier ${}^7\text{Li}$ isotopes during precipitation of both CaCO_3 polymorphs. This offset is consistent with the fractionation seen in other studies (*Marriott et al., 2004a; Marriott et al., 2004b; Gabitov et al., 2011; Day et al., 2021; Fuger et al., 2022*). However, the Li isotope fractionation between aragonite samples and solution observed in the present study is on the order of about -16‰ , which is slightly larger than the values reported in previous studies.

Marriott et al. (2004a) reported Li isotope fractionation of about -3‰ in calcite and -12‰ in aragonite with respect to the experimental solution. *Day et al. (2021)* reported an average ${}^7\epsilon_{\text{solid-solution}}$ of -8.17‰ for all inorganic calcite samples and *Gabitov et al. (2011)* reported ${}^7\epsilon_{\text{solid-solution}}$ values ranging from -10.44 to -7.67‰ for synthetic aragonite. Fractionation between inorganic calcite and a simple solution in *Marriott et al. (2004b)* showed an average of -8.5‰ . *Fuger et al. (2022)* reported an average fractionation between calcite samples and parent fluid under similar solution pH values of -2.76‰ (See **Figure A2** in Appendix).

Despite both polymorphs favoring ^6Li , there is a dramatic difference in the magnitude of isotope fractionation with respect to solutions between calcite and aragonite samples (a difference of approximately 13‰ to 14‰). *Marriott et al. (2004a)* similarly found a $^7\epsilon_{\text{solid-solution}}$ offset of only up to $\sim 9\%$ between inorganic calcite and aragonite. This is likely due to the fact that *Marriott et al. (2004a)* used calcite seeds to initiate precipitation for both calcite and aragonite samples. In their aragonite experiments, they used synthetic seawater with $[\text{Mg}^{2+}]$ and $[\text{SO}_4^{2-}]$ reflecting that of modern seawater to create a condition favorable for aragonitic CaCO_3 precipitation (as discussed in Section 3.2). But in their calcite precipitation experiments, concentrations of the respective ions were reduced ($[\text{Mg}^{2+}]$ at 10% that of seawater and no $[\text{SO}_4^{2-}]$) to ensure their experimental condition was more favorable for calcite precipitation. While such an adjustment of synthetic seawater chemical composition should favor precipitation of aragonite (*Bots et al., 2011*), it is possible that a mixture of calcite and aragonite overgrowth precipitated due to a templating effect from the calcite seeds used in their experiments. Since calcite is more enriched in ^7Li than aragonite (e.g., see **Figure 5**), the aragonite $\delta^7\text{Li}$ values in *Marriott et al. (2004a)* may be biased towards a higher value due to inclusion of some calcite that co-precipitated with aragonite.

Day et al. (2021) also reported $\delta^7\text{Li}$ values for calcite, high-Mg calcite, and aragonite samples, stating that no difference in fractionation was observed between the polymorphs. However, there were some key differences in the methodology of CaCO_3 precipitation used in *Day et al. (2021)*, which produced inorganic speleothem-analogues using a drip-method over calcite seeds. Additionally, the high-Mg calcite and aragonite samples were not precipitated under the same conditions as the calcite samples, making it difficult to identify and separate potential controls on fractionation due to differences in mineralogy.

One possible explanation for the preferential uptake of ^6Li in both calcite and aragonite is due to kinetic isotope effects arising from the large mass difference between ^6Li and ^7Li . Molecular dynamics simulations suggest that the desolvation rates of metal cations have a relatively strong mass dependence, with the lighter isotope having a faster desolvation rate and greater tendency to attach to the mineral surface rate, and thus being preferentially incorporated into a precipitating mineral (*Hoffman et al. 2012*). The large mass difference ($\sim 1\%$) between the two isotopes would result in ^7Li having a significantly slower desolvation rate than ^6Li . At high rates of precipitation, this can cause a fractionation effect that results in CaCO_3 with a lower $\delta^7\text{Li}$

value relative to that of the parent solution. However, as shown in **Figure 7**, there was no relationship between the observed Li isotope fractionation and CaCO₃ precipitation rates in both calcite and aragonite experiments. Moreover, kinetic isotope effects cannot adequately explain the consistent $\delta^7\text{Li}$ difference of ~13‰ observed between the two CaCO₃ polymorphs. Therefore, it is unlikely that fractionation revealed in the present study is dominated by kinetic isotope effects.

It is likely that the differences in the Li isotope fractionation between calcite and aragonite observed in the present study and *Marriott et al. (2004a)* are due to mineralogy, primarily the differences in mineral structure and the coordination of Li within the crystal lattice. It is likely that in aqueous solutions, Li is strongly bound with four water molecules within the first hydration shell (*Yamaji et al., 2001*). Theoretical estimations of the vibration frequencies of Li in various hydration structures suggest this tetrahedral coordination is the most stable for Li and it is usually more weakly bound at higher coordination numbers (*Yamaji et al., 2001*). Li is often incorporated into minerals at higher coordination numbers with weaker bond strengths than in aqueous solution, which explains the preferential uptake of ⁶Li observed in carbonate and clay minerals (*Huh et al., 1998; Penniston-Dorland et al., 2017*).

In aragonite, it is thought that Li substitutes for the Ca²⁺ sites, which are in ninefold coordination with the oxygen atoms within the crystal structure (*Morse et al., 2007*). In contrast, Ca²⁺ sites in calcite are bound in a sixfold coordination (**Figure 8**). However, there is some controversy in how alkali metals, including Li, are incorporated into the calcite structure. It was previously thought that alkali metals are not incorporated in the Ca²⁺ sites in calcite, but rather interstitially (*Busenberg & Plummer, 1985; Okumura & Kitano, 1986; Mucci, 1988*). More recent studies, however, suggest that alkali metals, such as Na⁺, may in fact be incorporated into the Ca²⁺ sites (*Yoshimura et al., 2007*). However, it should also be cautioned that Li incorporation into the Ca²⁺ site for aragonite or calcite does not guarantee that the coordination number of Li⁺ will be the same as Ca²⁺ due to differences in their ionic size and charge. Regardless, it is likely that Li is bound in calcite and aragonite at higher coordination numbers than presumably the most stable fourfold (tetrahedral) coordination of Li in aqueous solution. Under equilibrium conditions, there is a tendency for the heavier isotope (e.g., ⁷Li) to preferentially accumulate in compounds where it is more strongly bound (*Bigeleisen, 1965*). Strictly speaking, this notion applies to covalent bonds. However, it should not be unrealistic to

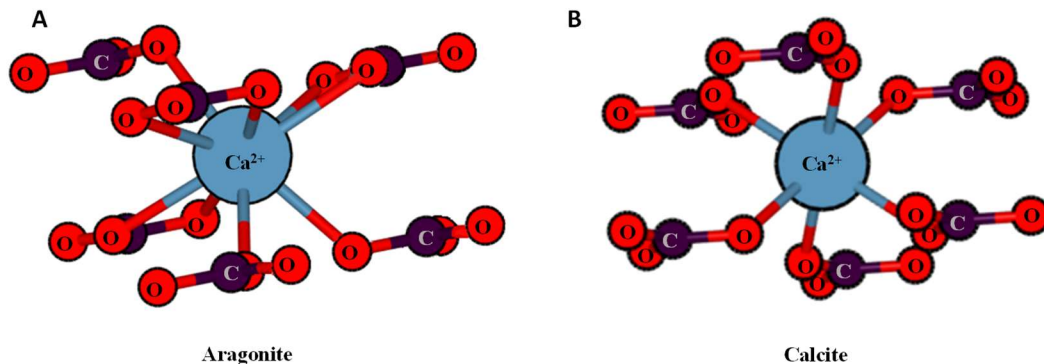


Figure 8: Aragonite and Calcite Ca^{2+} Coordination

Coordination of Ca^{2+} site (large blue atom) in the aragonite (A) and calcite lattice (B), as noted by the numbers of bond formation with oxygen atoms (small red atoms) in CO_3^{2-} molecules (carbon: small dark-purple atoms). In aragonite, Ca^{2+} is bound with 9 oxygen atoms, in calcite Ca^{2+} is bound with 6 oxygen atoms. Images were produced using VESTA software (Momma & Izumi, 2011).

assume that the concept also applies to other types of chemical bonds, including presumably ionic bonds formed for/by Li within the calcite and aragonite structure. Thus, the fractionation offset observed between the two polymorphs may be due to a difference in the coordination number of Li between calcite (lower) and aragonite (higher), which results in Li bound more strongly in calcite than in aragonite. **Figure 9** presents an illustration of the relationship between coordination number with Li bond strength and its influence on the fractionation of Li isotopes, assuming the coordination number for Li increases from water to calcite to aragonite. A study by Gussone *et al.* (2005) reported a similar trend with Ca isotopes. Calcite and aragonite were observed to incorporate less of the heavy isotope (^{44}Ca) from aqueous Ca^{2+} in solution due to the Ca-O bonds of aqueous Ca with water molecules being the most stable. The Ca-O bonds in calcite are stronger than aragonite, which is reflected in the larger fractionation observed in aragonite than calcite (i.e., calcite incorporates more ^{44}Ca than aragonite). While the resulting Ca-O bond strength is not directly reflected by the Ca coordination number, the pattern of preferential uptake of the heavy isotope (^{44}Ca) due to Ca-O bond strength increasing from aragonite to calcite to water is consistent with the case for Li isotopes. It is likely that this holds for Li, with the preferential uptake of the heavy isotope (^7Li) being related to bond strength increasing from aragonite to calcite to water. However, this interpretation is speculative, as the actual coordination environment of Li in calcite and aragonite has not been determined.

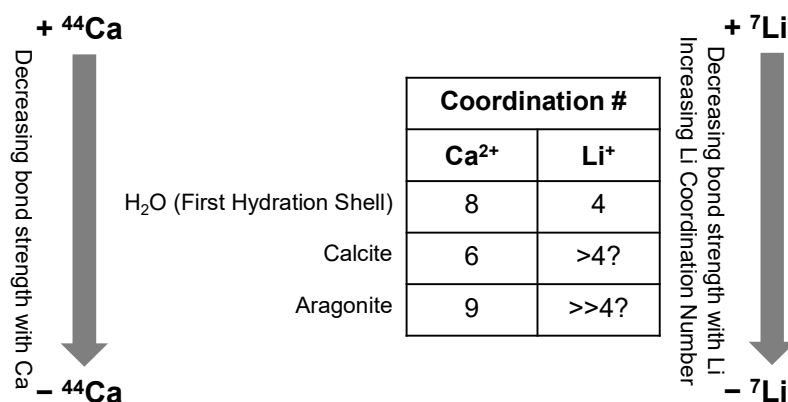


Figure 9: Relationship between Li Coordination and Isotope Fractionation

Relationship between coordination number of Ca²⁺ and Li⁺ in water, calcite, and aragonite and the Li fractionation as a result of bond strength. The + ⁷Li signifies greater incorporation of ⁷Li and – ⁷Li refers to less ⁷Li incorporation. This relationship assumes that coordination number of Li increases from water to calcite to aragonite. Given that coordination of Li in calcite and aragonite is yet to be directly examined analytically, the coordination numbers for Li in calcite and aragonite are denoted by “?”. Reported coordination of Ca²⁺ in water is from a molecular dynamic simulation study by *Jalilehvand et al. (2001)*.

4.2 Controls on Li Isotope Fractionation in CaCO₃ with Respect to Solution

4.2.1 Calcite

The isotopic offset between calcite and aragonite suggests some control on fractionation due to mineralogical structural differences in Li coordination number and bond strength, which are indicative of equilibrium isotope effects. However, uncertainties in the mechanisms for Li incorporation in calcite make it difficult to constrain any potential equilibrium controls. It is necessary to understand how Li is being incorporated (e.g., as a free ion or as part of a complex) and where Li is being incorporated (e.g., interstitially or in the Ca²⁺ site) in the calcite structure in order to confidently assess equilibrium effects.

There is disagreement in the observed effect of pH on the ⁷ε_{solid-solution} value of calcite between the present and prior studies. While the present study observed a negative correlation between the ⁷ε_{solid-solution} value of calcite and pH, both *Füger et al. (2022)* and *Seyedali et al. (2021)* noted a positive correlation. There are a few possible explanations for these disagreements. First, there was a difference in the experimental design between the present study and *Seyedali et al. (2021)*, in which pH drifted over the course of the experiment as their calcite samples were transformed from a vaterite precursor. Due to these differences, it is possible that the results may not be directly comparable. However, the experimental design in *Füger et al.*

(2022) and the present study had more similarities, both maintaining a relatively constant pH and precipitating calcite over seeds. Thus, methodological differences do not fully explain the conflicting results.

There is also a large difference in pH ranges tested. Both *Seyedali et al. (2021)* and *Füger et al. (2022)* tested a larger range of solution pH values than was conducted in the present study (pH range of 8.0 to 8.4), with *Füger et al. (2022)* conducting experiments across a pH range of 6.3 to 9.5 and *Seyedali et al. (2021)* across a pH range of 7.0 to 9.2. It is possible that the range of solution pH values tested in the present study does not fully capture the effect of solution pH on Li isotope fractionation across a larger range. Changing solution pH significantly impacts the degree of CaCO₃ saturation (SI_{Calcite}) and thereby precipitation kinetics. This warrants further consideration of calcite precipitation rates when comparing experimental results across different studies. *Füger et al. (2022)* reported a strong, negative correlation between precipitation rate and the ${}^7\epsilon_{\text{solid-solution}}$ value of calcite, whereas the present study observed none. The study by *Day et al. (2021)* also observed a negative relationship between rate and the ${}^7\epsilon_{\text{solid-solution}}$ value of CaCO₃ samples. One key difference is that the present study precipitated calcite at significantly more rapid rates ($10^{-6.5}$ to $10^{-5.4}$ mol/m²/s) compared to those in *Füger et al. (2022)* ($10^{-8.1}$ to $10^{-7.7}$ mol/m²/s) (see **Figure 10**). The rate of biogenic calcite precipitation by foraminifera can vary (discussed further in section 4.5), however tends to be quite rapid. A study by *Carpenter & Lohmann (1992)* approximated biogenic calcification rates in foraminifera to be around $10^{-4.77}$ mol/m²/s, suggesting rapid inorganic calcite precipitation rates are an appropriate analogue to foraminifera growth (*Zeebe & Sanyal, 2001*).

The surface kinetic model developed by *DePaolo (2011)* describes how variations in precipitation rate can influence whether isotopic fractionation will be dominated by kinetic or equilibrium effects. When CaCO₃ minerals grow very slowly (i.e., close to the chemical equilibrium), isotope fractionation between CaCO₃ minerals and solution is driven by equilibrium isotope effect with practically no influence of kinetic isotope effects related to mechanical processes (e.g., mass transport, diffusion, ion desolvation, etc.) that should be sensitive to the mass difference between the light and heavy isotopes.

Füger et al. (2022) applied the surface kinetic model of *DePaolo (2011)* and argued that the strong dependence of ${}^7\epsilon_{\text{solid-solution}}$ to calcite precipitation rates shown in their experimental results is attributable to kinetic isotope effects. Their model fitting to the experimental data

indicates minimal fractionation driven by kinetic isotope effects at R below $10^{-7.7}$ mol/m²/s. But as R increases from $10^{-7.7}$ to $10^{-7.2}$ mol/m²/s, the kinetic isotope effects will be more strongly pronounced, which results in a decrease in the $\delta^7\text{Li}$ value of precipitating calcite. Eventually, $\text{Log}_{10}R$ will increase and reach a “kinetic limit”, as described in *DePaolo (2011)*, where fractionation will remain relatively constant.

Assuming the model fitting by *Füger et al. (2022)* is correct, the positive correlation between calcite ${}^7\epsilon_{\text{solid-solution}}$ values and pH observed in the studies by *Füger et al. (2022)* and *Seyedali et al. (2021)* may be due to weakly pronounced kinetic effects as calcite samples were precipitated at R slower than $10^{-7.8}$ mol/m²/s. (Note: *Seyedali et al. (2021)* reported 0.1 g of calcite was grown in 5-400 days, although rates were not specified). This would suggest that the negative relationship observed in the present study could be due to complications from kinetic effects, with ${}^7\epsilon_{\text{solid-solution}}$ values decreasing at higher pH due to the increasing precipitation rate. It is worth noting that in the present study, samples precipitated during the combined $[\text{Ca}^{2+}]/\text{pH}$

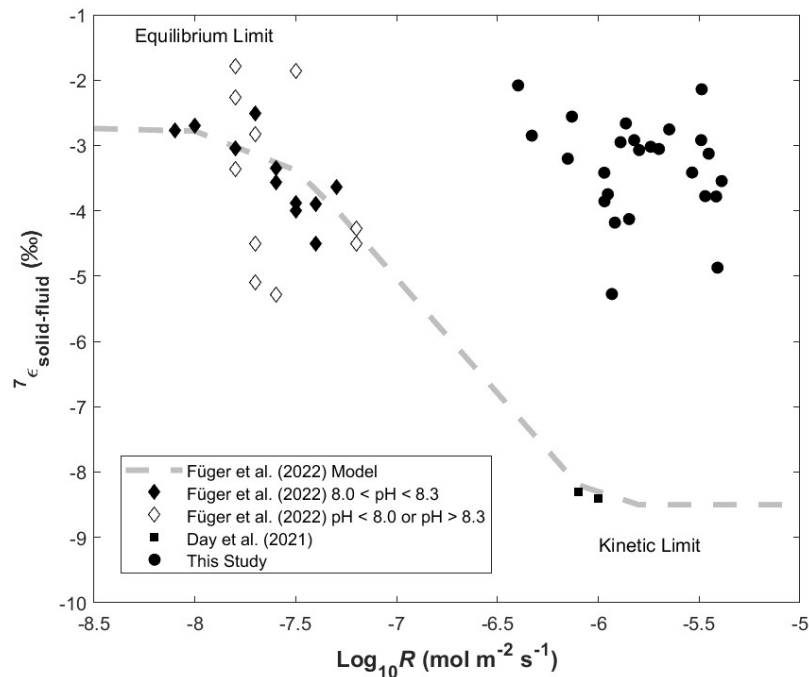


Figure 10: *Füger et al. (2022)* Model

A comparison of the model relating fractionation to precipitation rate proposed by *Füger et al. (2022)* with data from (◆) *Füger et al. (2022)* (within pH range of 8.0 to 8.3), (◇) *Füger et al. (2022)* (with pH below 8.0 or above 8.3), (■) *Day et al. (2021)*, and (●) calcite samples from the present study.

parameter series (consistent kinetic effects) also observed a positive relationship between ${}^7\epsilon_{\text{solid-solution}}$ of calcite and pH. But overall, the model fit by *Füger et al. (2022)* is clearly inconsistent with the experimental data from the present study (see **Figure 10**).

The model fit by *Füger et al. (2022)* suggests a consistent offset between calcite and solution of approximately -9% when precipitation rate reaches the kinetic limit. Based on this model, the rate of precipitation for calcite samples in the present study (R above $10^{-7.2}$ mol/m²/s) is at the kinetic limit, and the expected Li isotope fractionation should be around -9% . However, samples produced in the present study had a fractionation of only $-3 \pm 1.0\%$ between calcite and the solution. The model fits the data reported by *Füger et al. (2022)* and *Day et al. (2021)* reasonably well, although it is important to note that *Day et al. (2021)* used an entirely different methodological approach for calcite precipitation (producing inorganic speleothem-analogues), so the two studies are not directly comparable. Despite $\text{Log}_{10}R$ being reported in the study (which is necessary for surface kinetic modeling), it is unclear if the reported fractionation (approximately -8%) is consistent with results from other studies producing inorganic foraminifera-analogues. *Marriott et al. (2004b)* reported calcite precipitates with a fractionation of -8.5% from the solution. However, they did not measure and/or explicitly report the $\delta^7\text{Li}$ value of the experimental solution, but rather they stated that $\delta^7\text{Li}$ value of dissolved Li in their experimental solutions was matched to LSVEC (i.e., $\delta^7\text{Li} = 0\%$ for their experimental solution). But it is uncertain how this was possible, given that LiCl was used as the Li source for their experimental solution and that Li_2CO_3 represents the chemical form of the LSVEC standard (*Flesch et al., 1973*). This causes some uncertainty in the reported fractionation. Additionally, *Marriott et al. (2004b)* does not report sample precipitation rates, making it difficult to compare with the *Füger et al. (2022)* model. With such variability in experimental methods across studies and a lack of available rate data, it is difficult to confidently constrain the maximum Li isotope fractionation between calcite and solution. Comparing the data reported by *Füger et al. (2022)* and results from the present study which used similar methods (i.e., a seeded method to precipitate foraminifera-analogous inorganic calcite), there is no clear relationship between precipitation rate and fractionation. While additional studies systematically manipulating a larger range of precipitation rates may provide further insight on possible kinetic fractionation effects, the current results from this study suggests Li fractionation between calcite and solution is dominated by equilibrium controls, with minimal or no influence from kinetic effects.

4.2.2 Aragonite

Unfortunately, there are few studies on inorganic aragonite with which to compare potential equilibrium or kinetic isotope effects. *Marriott et al. (2004a)* found no relationship between the ${}^7\varepsilon_{\text{solid-solution}}$ value of aragonite and the salinity of the synthetic seawater used in their experiments. Both *Gabitov et al. (2011)* and the present study found no significant relationship between precipitation rate and the $\delta^7\text{Li}$ value of aragonite. However, in the present study, there was a statistically significant positive relationship between the ${}^7\varepsilon_{\text{solid-solution}}$ value of aragonite with both $[\text{DIC}]$ and $[\text{Ca}^{2+}]$, indicating more ${}^7\text{Li}$ was incorporated at higher solution $[\text{DIC}]$ and $[\text{Ca}^{2+}]$ (both leading to an increase in $\text{Log}_{10}R$). This is opposite of what can be expected for the kinetic isotope effects, which usually results in preferential uptake of the lighter isotope (i.e., ${}^6\text{Li}$) with faster precipitation rates. The results from this study suggest that equilibrium effects are the primary control on Li fractionation in aragonite, with little or no influence from kinetic effects. However further studies on aragonite are necessary to better understand these potential controls.

4.3 Controls on Li/Ca

There is a statistically significant, albeit very weak, positive correlation between the precipitation rate and D_{Li} for both calcite and aragonite in the present study, which is consistent with observations for calcite in *Füger et al. (2019)* and aragonite in *Gabitov et al. (2011)*. *Füger et al. (2019)* suggests a strong kinetic dependence on the incorporation of Li in calcite. Previous studies on the mechanisms of trace element incorporation in calcite suggest alkali metals are incorporated interstitially, which is facilitated by distortion or defects in the crystal structure from Mg incorporation (*Okumura & Kitano, 1986; Mucci, 1988*). The presence of these crystal defects increases with the rate of precipitation, resulting in an increase in alkali metal incorporation (*Busenberg & Plummer, 1985; Okumura & Kitano, 1986; Mucci, 1988*).

Figure 11 shows the Li/Ca relative to Mg/Ca of the solid calcite and aragonite samples (**Table A5**, see Appendix), showing a strong correlation ($R^2 = 0.58$ $p < 0.01$ for calcite; $R^2 = 0.58$ $p < 0.01$ for aragonite, respectively) between the incorporation of Mg with the incorporation of Li for both calcite and aragonite. *Gabitov et al. (2011)* also observed an increase in both Mg/Ca and Li/Ca incorporation in aragonite with higher rates of precipitation. If Mg facilitates the incorporation of Li, that may explain the strong relationship between Mg/Ca and Li/Ca ratios in calcite.

However, as previously discussed, more recent studies propose that alkali metals are incorporated into the calcite lattice structure via direct substitution with Ca^{2+} (*Yoshimura et al., 2007*). If this is the case, the relationship between Mg/Ca and Li/Ca possibly reflects an increase in the overall incorporation of trace metals due to growth rate. The effect of growth rate on trace metal incorporation has been explored using the growth entrapment model (*Watson and Liang, 1995; Watson, 2004*). This model suggests that during calcite precipitation, trace elements are enriched in the crystal surface. At high rates of crystal growth, these trace elements are more likely to become entrapped. These surface kinetic effects can vary strongly with growth rates, suggesting that Li incorporation in CaCO_3 strongly depends on precipitation rate.

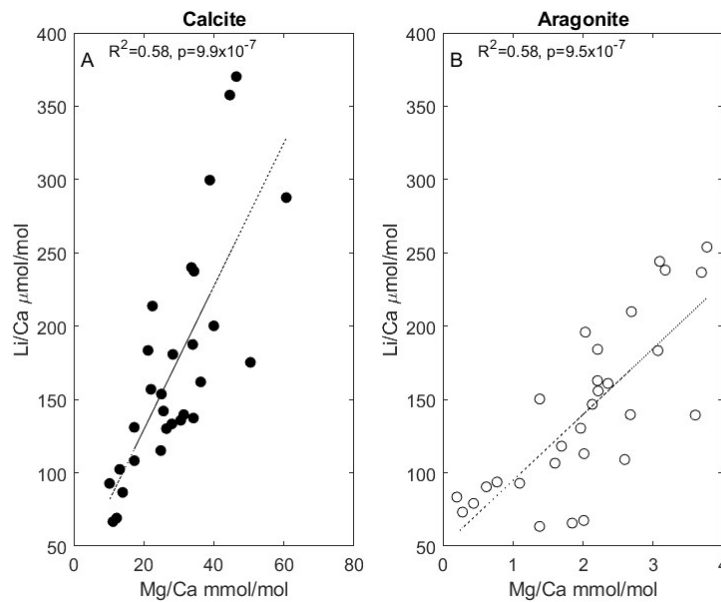


Figure 11: Mg/Ca vs Li/Ca

Li/Ca ratios as a function of Mg/Ca ratios for calcite (A) and aragonite (B) overgrowth. Note the differences in the Mg/Ca ratios (x-axis) between calcite and aragonite.

This is consistent with the positive correlation between $[Ca^{2+}]$ and D_{Li} observed for calcite, as the rate of precipitation for the calcite samples increased with higher $[Ca^{2+}]$ in the experimental solution. However, this was not observed with the pH or [DIC] series, which had a similar change in precipitation rate as the $[Ca^{2+}]$ series. Additionally, in the combined $[Ca^{2+}]$ /pH parameter series where experiments were conducted at a similar precipitation rate, there was a significant relationship between D_{Li} of calcite samples and pH (negatively correlated: **Figure 6D**) and $[Ca^{2+}]$ (positively correlated: **Figure 6C**). If precipitation rate is a major control on the Li/Ca ratio of calcite, these results are unexpected, as each of the $[Ca^{2+}]$ /pH experiments were conducted at a similar saturation index so that the precipitation rate across experimental solution parameters would be the same.

One possible explanation for this is an inconsistent precipitation rate during experimental runs, resulting in variable D_{Li} data. During most experiments, the rate of titrant addition accelerated from the time of initial seed addition to the termination of experiments (**Figure A3**, see Appendix), reflecting an increasing rate of $CaCO_3$ precipitation with time. This is likely due to an increase in the total surface area as individual $CaCO_3$ crystals grow in size with time due to continuous deposition of the new overgrowth over the seeds. Despite this increase in the total $CaCO_3$ surface area, some titration plots featured an approximately linear titrant addition, indicating a relatively stable precipitation rate (**Figure A4**, see Appendix). This was particularly the case in the aragonite precipitation experiments. However, maintaining a steady pace of titration over the course of an experimental run was a major challenge, likely due to the presence of Mg in the experimental solution (discussed in further detail in section 4.4). During low end-member (pH = 8.0, [DIC] = 1.575 mM, and $[Ca^{2+}]$ = 2.625 mM) experiments, there were more extreme difference in the rate of titrant addition between the start and end of the experiments (sometimes increasing by 200% to 300%), indicating a dramatic acceleration in precipitation rate over the course of an experimental run. While the overall average precipitation rate during the combined $[Ca^{2+}]$ /pH series was similar to that of the controls, there was variation in the steadiness of precipitation rate across parameters (See **Figure A4** in Appendix). Samples precipitated at pH = 8.0 and $[Ca^{2+}]$ = 7.875 mM had a steady precipitation rate, relatively unchanged from start to end of the experiment. However, in the experiments performed at pH = 8.4 and $[Ca^{2+}]$ = 2.625 mM, the initial precipitation rate almost doubled by the end of the experiment. If the rate of mineral formation is a major control on the incorporation of Li, this

temporal variability in the calcite precipitation rate within a given experimental run could explain the observed variations in D_{Li} values of replicate samples precipitated under the same condition.

Marriott et al. (2004a) proposed that since Li and Ca are in competition with each other for placement at the Ca^{2+} site within the aragonite crystal lattice, the most important control on the Li/Ca ratio of aragonite would be the Li/Ca ratio of the solution. If this holds, there should be a decrease in the D_{Li} value of aragonite samples with an increase in the $[\text{Ca}^{2+}]$ of the solution. Despite this expectation, the present study observed an opposite pattern. There was a positive correlation between D_{Li} and the $[\text{Ca}^{2+}]$ of the experimental solution observed for both calcite and aragonite. Additionally, there was no significant trend between aragonite D_{Li} values and $[\text{Ca}^{2+}]$ or pH in the combined parameter series, which would be expected if the Li/Ca ratio of the solution is the primary control on the Li/Ca ratio of aragonite. This, along with the relationship between precipitation rate and the D_{Li} values for aragonite observed both in the present study and in *Gabitov et al. (2011)*, suggests that the precipitation rate is the primary control on Li incorporation in aragonite.

4.4 Effects of Mg^{2+} on Precipitation

As mentioned above, one of the major challenges in the present study was to maintain a steady and consistent pace of titration (i.e., CaCO_3 precipitation rate) over the course of the experiments, particularly for calcite samples. During most calcite experiments, the pace of titration increased somewhat exponentially from the beginning to end of the experiment (**Figures A3 and A4** in Appendix). It is likely that precipitation of the CaCO_3 samples was influenced by the presence of Mg in the experimental solution, which has been observed to interfere with precipitation of calcite (*Berner, 1975; Mucci & Morse, 1983; Morse et al., 2007; Pan et al., 2021*).

Mg in solution can affect calcite precipitation rate in a number of ways. One way is through the formation of Mg^{2+} and CO_3^{2-} ion pairs, which can reduce the amount of free CO_3^{2-} available for CaCO_3 precipitation (*Zeebe & Sanyal, 2002*). This may have a greater effect on precipitation at lower pH and [DIC], where there is less initial free CO_3^{2-} in the solution. The incorporation of Mg into the calcite crystal lattice can also change the crystal morphology and interfere with precipitation by increasing mineral solubility (*Berner, 1975; Mucci & Morse,*

1983; Zeebe & Sanyal, 2002). Under higher solution $[Mg^{2+}]$, there is more incorporation of Mg^{2+} in calcite and the solubility constant of calcite (K_{sp}^*) increases, which ultimately results in a lower saturation state and lower rate of calcite precipitation (Mucci & Morse, 1984). However, with low amounts of Mg^{2+} incorporation (below ~ 5 mol% $MgCO_3$), calcite actually becomes less soluble than pure calcite (Morse *et al.*, 2007). This decrease in K_{sp}^* in low Mg-calcites (**Figure A5** in Appendix) inevitably causes an increase in both saturation state and thus precipitation rate without making any change to solution chemistry (e.g., $[Ca^{2+}][CO_3^{2-}]$). Over the course of the precipitation experiments, the calcite samples transition from almost pure calcite (seed material) to a low Mg-calcite due to Mg incorporation from experimental solution to the new $CaCO_3$ overgrowth. This may explain the almost exponential increase in precipitation rate (**Figure A3** in Appendix) observed during the calcite experiments.

Another factor contributing to inconsistencies in precipitation rate may be that the precipitation of calcite in Mg-bearing solutions can also result in notable geometric and morphological changes in the rhombohedral shape of the original calcite seeds. **Figure 4** shows the calcite seed crystal (**4C**) juxtaposed with the calcite post-precipitation (**4D**) during one of the control experiments. The calcite seeds have smooth surfaces and a well-defined rhombohedral structure, whereas the post-precipitation calcite samples show apparent deformation of the rhombohedral shape and surface roughness due to the presence of “growth islands”. Similar irregular shapes of calcite precipitated in the presence of Mg have been observed in other studies (Berner, 1975; Pan *et al.*, 2021). These surface topographic features resulted in a non-systematic increase in total surface area with time across replicate experiments performed at a given condition. This variability in surface area and overgrowth, along with changes in K_{sp}^* due to some incorporation of Mg, is likely the cause of uncontrollable precipitation rate, especially during the calcite experiments, which may then have significantly influenced the Li/Ca ratios of the overgrowth samples.

4.5 Comparison with Culture Experiments

The isotopic fractionation of Li in inorganic calcite and aragonite are similar to those observed in biogenic $CaCO_3$, with a preferential incorporation of 6Li . Marriott *et al.* (2004b) observed aragonitic coral samples (*Porites*) with a fractionation of approximately -11‰ from the growth solution. The $CaCO_3$ tests of the foraminifera *A. lessonii* cultured in Roberts *et al.*

(2018) had isotopic offsets ranging from approximately -1 to -4‰ with respect to $\delta^7\text{Li}$ of seawater used in their culture experiments. In contrast to these studies, *Vigier et al. (2015)* reported the $\delta^7\text{Li}$ value of calcitic CaCO_3 precipitated by *A. lobifera* was similar to that of seawater (some samples were reported as having $\delta^7\text{Li}$ values above 31‰), suggesting CaCO_3 precipitation does not favor ^6Li . This is inconsistent with the notable ^7Li depletion seen in inorganic and biogenic CaCO_3 as repeatedly mentioned above. However, as caveats, it should be noted that *Vigier et al. (2015)* did not measure or report the $\delta^7\text{Li}$ values of seawater used in their culture experiments. Furthermore, they analyzed foraminiferal $\delta^7\text{Li}$ and Li/Ca values using an ion microprobe (more commonly known as secondary ion mass spectrometer), which is a somewhat unconventional approach in comparison to the ICPMS analyses after Li separation and purification from the CaCO_3 matrix using the cation exchange resin (see Section 2.6) used in other studies, including the present one.

Roberts et al. (2018) observed a strong inverse relationship between pH and the $\delta^7\text{Li}$ value of biogenic calcite in cultured *A. lessonii* tests, whereas *Vigier et al. (2015)* found no relationship between the $\delta^7\text{Li}$ value of biogenic calcite in *A. lobifera* tests with pH. Conversely, *Roberts et al. (2018)* observed no trend with $[\text{DIC}]$, whereas *Vigier et al. (2015)* observed a strong positive correlation with $[\text{DIC}]$. Additionally, there were some discrepancies with the Li/Ca ratio data across the two studies. *Roberts et al. (2018)* and *Vigier et al. (2015)* both observed no trend between pH and the Li/Ca ratio. But *Roberts et al. (2018)* observed a positive correlation between Li/Ca and $[\text{DIC}]$, as opposed to a negative trend found by *Vigier et al. (2015)*. A culture study by *Allen et al. (2016)* studied trace element incorporation in various planktic symbiont-bearing foraminifera species, observing a trend of decreasing D_{Li} with increasing growth rate (except in non-symbiont-bearing species *Globigerinoides bulloides*).

While some inorganic studies (*Day et al., 2021; Seydali et al., 2021; Fuger et al., 2022*) suggest the importance of precipitation rate on determining the Li isotopic and elemental incorporation in calcite, it is unclear how this relationship may apply to calcification by marine organisms, particularly with the complication of biological vital effects. *Allen et al. (2016)* reported an offset in the D_{Li} value between species, suggesting that there is some biological control on Li incorporation. As neither *Roberts et al. (2018)* nor *Vigier et al. (2015)* report growth rates for their studies, it is difficult to identify the potential role of calcification rate versus biological effects influencing the observed Li incorporation. The study by *Carpenter &*

Lohmann (1992) approximated biogenic calcification rates in foraminifera to be around $10^{-4.77}$ mol/m²/s. Culture studies that grew planktonic foraminifera species *Orbulina universa* found variable growth rates: $10^{-8.8}$ to $10^{-8.4}$ mol/m²/s (Haynes et al., 2017), $10^{-8.1}$ mol/m²/s (Allen et al., 2016), and $10^{-6.5}$ to $10^{-6.1}$ mol/m²/s (Holland et al., 2017). Additionally, a paper by Geerken et al. (2022) studied the growth rate of benthic foraminifera *Ammonia beccarii* and suggested that the biomineralization of CaCO₃ in benthic foraminifera can occur quite rapidly ($10^{-5.40}$ mol/m²/s).

Not considering complications due to vital effects, results from the present inorganic study suggests that under rapid precipitation rates within the range of $10^{-6.5}$ to $10^{-5.4}$ mol/m²/s, Li isotope fractionation in calcite is insensitive to rate changes. However, variability in growth rates across foraminifera species may play an important role in influencing the Li/Ca ratio of the calcitic tests. There is also some uncertainty in how sensitive Li isotope fractionation may be to rate changes under slower precipitation rates. This signifies the importance of constraining foraminifera calcification rates and its relationship to Li incorporation in order to confidently use the Li/Ca and $\delta^7\text{Li}$ values of foraminiferal CaCO₃ as a proxy tool. Complications due to vital effects will also need to be considered. However, given the rapid rates of CaCO₃ precipitation reported for foraminifera species (Carpenter & Lohmann, 1992; Holland et al., 2017; Geerken et al., 2022), the results from this study are promising for the use of Li isotopes in calcitic foraminifera tests to trace past silicate weathering.

5. SUMMARY & CONCLUSIONS

In the present study, individual parameter precipitation experiments manipulated pH, [DIC], and [Ca²⁺] of the experimental parent solution. There was a significant negative relationship between pH and the Li isotope fractionation for calcite. For aragonite, there was a significant positive relationship between fractionation and [DIC] and [Ca²⁺]. There was also a negative relationship between pH and the fractionation of aragonite samples significant at the 90% confidence level. Experiments in the combined [Ca²⁺]/pH parameter series were conducted at a similar precipitation rate (constant kinetic effects) and indicated a significant positive relationship between the pH of the experimental solution and Li isotope fractionation for calcite but not aragonite samples. It is important to note that while these relationships were statistically significant, they were weak and resulted in a minimal overall effect (less than 2-3‰) on the

${}^7\epsilon_{\text{solid-solution}}$ value within the range of tested solution chemistry parameters. There was a consistent offset of approximately 13‰ between the ${}^7\epsilon_{\text{solid-solution}}$ values for calcite and aragonite. No significant relationship was observed between precipitation rate and fractionation for either calcite or aragonite.

The results of the present study are broadly consistent with previous observations of calcite and aragonite samples having a lower $\delta^7\text{Li}$ value relative to that of the parent solution. This supports the notion that carbonate minerals preferentially incorporate ${}^6\text{Li}$ over ${}^7\text{Li}$, likely due to the tetrahedral coordination of Li with water in aqueous solutions resulting in the most stable bonds. There seems to be a relationship between Li coordination number within a structure and the resulting bond strength. Lower Li coordination numbers result in stronger bonds, leading to preferential uptake of ${}^7\text{Li}$. Conversely, as coordination number increases, bond strength decreases and less ${}^7\text{Li}$ is incorporated. Although the actual coordination numbers for Li in calcite and aragonite are not well known at this stage, if Li substitutes for Ca in the lattice and directly interacts with neighboring oxygen atoms of CO_3 in the calcite and aragonite structure, it is likely that Li has a lower coordination number in calcite than in aragonite. This leads to greater fractionation of Li isotopes in aragonite, as less ${}^7\text{Li}$ is incorporated due to weaker bond strengths within the aragonite crystal structure. While this mineralogical difference should be indicative of equilibrium isotope effects, the precipitation rate of CaCO_3 samples in the present study were comparatively more rapid than the range covered in other experimental studies. Thus, whether or not the data from the present study would reflect the full extent of the equilibrium isotope fractionation is still an open question.

A previous inorganic calcite study by *Füger et al. (2022)* reported a strong negative correlation between Li isotope fractionation in calcite and precipitation rate, which was attributed to kinetic isotope effects. However, the data from the present study show no apparent trend between Li isotope fractionation in calcite and precipitation rate (**Figure 7**). By combining the data from the present study and *Füger et al. (2022)*, which are both based on relatively similar experimental approach and methods, there seem to be no observable trend in Li isotope fractionation between calcite and solution as a function of $\text{Log}_{10}R$ spanning over almost three orders of magnitude. This suggests that kinetic isotope effects associated with Li incorporation during inorganic calcite precipitation are likely too small to resolve experimentally.

There is a positive relationship between precipitation rate and the Li/Ca ratios of both calcite and aragonite. This is consistent with the growth entrapment model, with faster precipitation rates resulting in the incorporation of both more Li and Mg. However, variability in precipitation rate across replicate runs due to presence of Mg in experimental solution make it difficult to identify additional controls on Li/Ca ratios of CaCO₃ samples in the present study.

Results from the present study have implications for the use of Li as a proxy tool for silicate weathering. The relationship between changes in solution chemistry parameters and isotope fractionation is weak, suggesting minimal effects due to carbonate chemistry. Inorganic calcite samples precipitated at rapid rates (above 10^{-6.5} mol/m²/s) suggest Li isotope fractionation is not sensitive to rate changes. The rate of foraminifera calcite precipitation is often quite rapid, although the reported rates across culture studies can be variable. While this is quite promising for the use of Li as a proxy tool, further studies to better constrain foraminifera precipitation rates as well as identify possible complications due to vital effects may be necessary to confidently use Li as tracer for past silicate weathering.

APPENDIX

Table A1: $\delta^{13}\text{C}$ and $\delta^{18}\text{O}$ values of BaCO_3 samples
 BaCO_3 samples used to preserve $\delta^{13}\text{C}$ value of ^{13}C -spiked Na_2CO_3 solution
for mass balance calculations

Sample	$\delta^{13}\text{C}$ (‰)		$\delta^{18}\text{O}$ (‰)	
BACO3 1A	118.3	± 0.020	-14.642	± 0.006
BACO3 1B	114.896	± 0.016	-14.502	± 0.009
BACO3 1C	113.919	± 0.011	-14.353	± 0.005
BACO3 2A	117.657	± 0.010	-14.743	± 0.013
BACO3 2B	116.86	± 0.011	-14.584	± 0.010
BACO3 2C	115.014	± 0.013	-14.358	± 0.006
BACO3 3A	129.835	± 0.022	-14.748	± 0.014
BACO3 3B	129.777	± 0.018	-14.697	± 0.012
BACO3 3C	128.612	± 0.014	-14.654	± 0.01
BACO3 4A	124.993	± 0.010	-14.89	± 0.013
BACO3 4B	125.74	± 0.015	-14.979	± 0.017
BACO3 4C	125.787	± 0.014	-14.701	± 0.015
BACO3 5A	75.056	± 0.017	-15.295	± 0.013
BACO3 5B	76.079	± 0.011	-15.479	± 0.01
BACO35C	75.264	± 0.008	-15.447	± 0.015

Table A2: Experimental Solution Concentrations
Sampled pre-precipitation and post-precipitation for experimental runs.

Sample	Solution (Pre)			Solution (Post)		
	[Ca] mM	[Mg] mM	[Na] mM	[Ca] mM	[Mg] mM	[Na] mM
Cont. Arag. 1	5.46	3.48	1.03	4.99	3.51	1.25
Cont. Arag. 2	5.47	3.50	1.03	4.76	3.47	1.18
Cont. Arag. 4	5.51	3.53	1.05	4.64	3.39	1.20
Cont. Arag. 5	5.41	3.46	1.01	4.92	3.45	1.21
Cont. Arag. 8	5.57	3.24	1.03	5.10	3.22	1.23
Cont. Arag. 9	5.62	3.55	1.07	5.16	3.43	1.12
Cont. Cal. 1	5.35	3.39	0.98	4.93	3.42	1.20
Cont. Cal. 2	5.53	3.51	1.03	4.94	3.47	1.23
Cont. Cal. 3	5.31	3.37	1.00	4.91	3.51	1.25
Cont. Cal. 4	5.51	3.48	1.03	5.06	3.50	1.25
Cont. Cal. 6	5.60	3.52	1.03	5.05	3.48	1.24
Cont. Cal. 8	5.37	3.40	1.01	4.81	3.41	1.27
Cont. Cal. 9	5.45	3.50	1.02	5.11	3.45	1.08
Cont. Cal. 11	5.28	3.39	1.02	5.15	3.46	1.14

Table A2 (Continued): Experimental Solution Concentrations

pH=8.4 Arag. 2	5.42	3.71	4.75	4.84	3.68	5.63
pH=8.4 Arag. 4	5.28	3.46	4.42	4.63	3.42	5.05
pH=8.0 Arag. 2	6.03	3.99	5.03	5.71	4.09	5.97
pH=8.0 Arag. 3	5.52	3.64	4.59	5.00	3.59	5.18
pH=8.4 Cal. 1	5.77	3.41	5.34	5.69	3.72	6.96
pH=8.4 Cal. 4	6.70	4.53	5.76	6.31	4.60	6.90
pH=8.0 Cal. 4	6.51	4.41	5.67	5.26	3.78	5.83
pH=8.0 Cal. 5	5.75	3.82	4.91	5.38	3.91	5.91
1.5x[DIC] Arag. 2	4.49	3.30	6.52	3.95	3.20	6.91
1.5x[DIC] Arag. 4	4.63	3.43	6.48	4.19	3.31	7.04
0.75x[DIC] Arag. 1	5.27	3.44	3.28	4.97	3.50	3.98
1.5x[DIC] Cal. 1	4.61	3.34	6.34	4.54	3.37	7.32
1.5x[DIC] Cal. 4	4.60	3.27	6.26	4.52	3.39	7.38
0.75x[DIC] Cal. 14	5.35	3.47	3.37	4.97	3.45	4.10
0.75x[DIC] Cal. 15	5.31	3.43	3.52	5.02	3.44	4.26
0.75x[DIC] Arag. 3	5.32	3.44	3.41	5.01	3.43	4.08
1.5x[Ca ²⁺] Arag. 2	7.15	4.98	4.28	6.92	5.04	5.07
1.5x[Ca ²⁺] Arag. 3	7.22	4.90	4.20	7.15	5.14	5.19
0.5x[Ca ²⁺] Arag. 1	2.78	1.78	4.67	2.30	1.75	5.41
0.5x[Ca ²⁺] Arag. 5	2.74	1.77	4.63	2.38	1.81	5.54
1.5x[Ca ²⁺] Cal. 1	7.10	5.01	4.53	6.79	4.97	5.27
1.5x[Ca ²⁺] Cal. 3	7.15	4.75	4.41	6.89	4.78	5.17
0.5x[Ca ²⁺] Cal. 3	2.70	1.74	4.60	2.42	1.77	5.44
0.5x[Ca ²⁺] Cal. 4	2.63	1.69	4.49	2.37	1.88	5.94
0.5x[Ca ²⁺]/pH=8.4 Arag. 2	2.70	1.49	4.74	2.23	1.43	5.27
0.5x[Ca ²⁺]/pH=8.4 Arag. 3	2.78	1.81	4.78	2.35	1.76	5.28
1.5x[Ca ²⁺]/pH=8.0 Arag. 1	7.39	5.02	4.85	6.42	4.22	3.72
1.5x[Ca ²⁺]/pH=8.0 Arag. 2	7.34	4.94	4.16	7.01	4.96	4.72
0.5x[Ca ²⁺]/pH=8.4 Cal. 2	2.73	1.76	4.60	2.39	1.67	4.86
0.5x[Ca ²⁺]/pH=8.4 Cal. 4	2.74	1.80	4.64	2.33	1.77	5.39
1.5x[Ca ²⁺]/pH=8.0 Cal. 1	7.32	4.76	4.24	7.21	4.97	5.05
1.5x[Ca ²⁺]/pH=8.0 Cal. 2	7.36	4.79	4.17	7.15	4.82	4.80

Table A3: $\delta^7\text{Li}$, ${}^7\epsilon_{\text{solid-solution}}$, and $\text{Log}R$ Data

Lithium isotope data for calcite and aragonite samples. ${}^7\epsilon_{\text{solid-fluid}}$ was calculated using the average $\delta^7\text{Li}$ value of the solution pre-precipitation.

Sample (Parameter/Run#)	$\delta^7\text{Li}$		${}^7\epsilon_{\text{solid-solution}}$		$\text{Log}_{10}\text{Rate}$ mol/m ² /s
	(‰)		(‰)		
Ctrl. Arag. 1	-3.28	±1.42	-18.14	±1.16	-6.42
Ctrl. Arag. 2	-2.56	±1.42	-16.42	±1.39	-6.45
Ctrl. Arag. 4	-2.51	±1.42	-18.19	±1.15	-6.36
Ctrl. Arag. 5	-1.70	±1.42	-15.22	±1.50	-6.38
Ctrl. Arag. 8	-2.77	±1.42	-17.98	±1.27	-6.43
Ctrl. Arag. 9	-3.39	±1.42	-17.92	±1.15	-6.54
Ctrl. Cal. 1	11.31	±1.42	-1.92	±1.18	-5.89
Ctrl. Cal. 2	11.19	±1.42	-3.17	±1.20	-5.80
Ctrl. Cal. 3	10.84	±1.42	-3.76	±1.21	-5.53
Ctrl. Cal. 4	11.24	±1.42	-3.07	±1.29	-5.74
Ctrl. Cal. 6	11.2	±1.42	-4.59	±1.61	-5.70
Ctrl. Cal. 8	11.51	±1.42	-0.43	±1.34	-5.65
Ctrl. Cal. 9	10.11	±1.42	-3.46	±1.33	-5.85
Ctrl. Cal. 11	10.84	±1.42	-4.45	±1.39	-5.97
pH=8.4 Arag. 2	-3.24	±0.80	-17.29	±1.19	-5.97
pH=8.4 Arag. 4	-2.31	±0.80	-16.38	±1.18	-6.05
pH=8.0 Arag. 2	-2.35	±0.80	-16.42	±1.26	-6.89
pH=8.0 Arag. 3	-2.09	±0.80	-16.16	±1.16	-6.93
pH=8.0 Arag. 9	0.07	±0.80	-14.03	±1.33	-6.94
pH=8.4 Cal. 1	9.36	±0.80	-4.87	±1.45	-5.41
pH=8.4 Cal. 4	10.71	±0.80	-3.54	±1.20	-5.39
pH=8.4 Cal. 5	10.47	±0.80	-3.78	±1.41	-5.42
pH=8.0 Cal. 4	11.71	±0.80	-2.56	±1.22	-6.13
pH=8.0 Cal. 5	11.05	±0.80	-3.2	±1.31	-6.15
1.5x[DIC] Arag. 2	0.17	±0.82	-13.93	±1.41	-6.07
1.5x[DIC] Arag. 4	-1.26	±0.82	-15.34	±1.41	-6.10
0.75x[DIC] Arag. 1	-2.69	±1.42	-16.75	±1.81	-6.56
0.75x[DIC] Arag. 3	-2.00	±0.82	-16.07	±1.41	-6.51
1.5x[DIC] Cal. 1	11.34	±0.80	-2.92	±1.41	-5.49
1.5x[DIC] Cal. 4	10.47	±0.80	-3.78	±1.41	-5.47
0.75x[DIC] Cal. 14	8.95	±0.80	-5.27	±1.41	-5.93
0.75x[DIC] Cal. 15	10.39	±1.42	-3.85	±1.82	-5.97
0.5x[Ca ²⁺] Arag. 1	-2.63	±1.42	-14.55	±1.81	-6.92
0.5x[Ca ²⁺] Arag. 5	-3.61	±1.42	-13.82	±1.81	-6.95
1.5x[Ca ²⁺] Arag. 2	-0.46	±0.82	-16.69	±1.41	-6.15
1.5x[Ca ²⁺] Arag. 3	0.28	±0.82	-17.66	±1.41	-6.13

Table A3 (Continued): $\delta^7\text{Li}$, $^7\epsilon_{\text{solid-fluid}}$, and $\text{Log}R$ Data

1.5x[Ca ²⁺] Cal. 1	12.13	±1.42	-2.14	±1.82	-5.49
1.5x[Ca ²⁺] Cal. 3	11.13	±0.80	-3.13	±1.41	-5.45
0.5x[Ca ²⁺] Cal. 3	12.19	±0.80	-2.08	±1.41	-6.40
0.5x[Ca ²⁺] Cal. 4	11.41	±1.42	-2.85	±1.82	-6.33
0.5x[Ca ²⁺]/pH=8.4 Arag. 2	-1.75	±0.82	-15.82	±1.41	-6.46
0.5x[Ca ²⁺]/pH=8.4 Arag. 3	-1.72	±0.82	-15.79	±1.41	-6.48
1.5x[Ca ²⁺]/pH=8.0 Arag. 1	-2.49	±0.82	-16.55	±1.41	-6.62
1.5x[Ca ²⁺]/pH=8.0 Arag. 2	-2.35	±0.82	-16.42	±1.41	-6.62
0.5x[Ca ²⁺]/pH=8.4 Cal. 2	11.60	±1.42	-2.66	±1.82	-5.86
0.5x[Ca ²⁺]/pH=8.4 Cal. 4	11.34	±0.80	-2.92	±1.41	-5.82
1.5x[Ca ²⁺]/pH=8.0 Cal. 1	10.06	±1.42	-4.18	±1.82	-5.92
1.5x[Ca ²⁺]/pH=8.0 Cal. 2	10.50	±0.80	-3.75	±1.41	-5.95

Table A4: Li/Ca ratio and D_{Li} Data
For Solid Samples and Solutions (Post-Precipitation).

<u>Sample</u> Parameter/Run #	<u>Solid</u>		<u>Solution</u>		D_{Li}	
	Li/Ca $\mu\text{mol/mol}$		Li/Ca $\mu\text{mol/mol}$			
Ctrl. Arag. 1	89.12	±0.53	59296.9	±0.03	0.0015	±1.2E-05
Ctrl. Arag. 2	75.24	±0.46	88591.8	±0.03	0.0008	±7.6E-06
Ctrl. Arag. 4	69.61	±0.42	57958.0	±0.03	0.0012	±1.1E-05
Ctrl. Arag. 5	72.84	±0.45	53366.8	±0.03	0.0014	±1.3E-05
Ctrl. Arag. 8	85.98	±0.53	79299.2	±0.03	0.0011	±9.2E-06
Ctrl. Arag. 9	79.33	±0.94	72689.2	±0.03	0.0011	±1.3E-05
Ctrl. Cal. 1	66.68	±0.42	59270.5	±0.03	0.0011	±1.1E-05
Ctrl. Cal. 2	68.41	±0.42	36437.4	±0.03	0.0019	±1.8E-05
Ctrl. Cal. 3	102.35	±0.42	39922.5	±0.03	0.0026	±1.6E-05
Ctrl. Cal. 4	83.07	±0.41	43315.8	±0.03	0.0019	±1.5E-05
Ctrl. Cal. 6	85.55	±0.44	57779.2	±0.03	0.0015	±1.1E-05
Ctrl. Cal. 8	86.61	±0.41	63652.3	±0.03	0.0014	±1.0E-05
Ctrl. Cal. 9	69.13	±0.86	82726.7	±0.03	0.0008	±1.1E-05
Ctrl. Cal. 11	92.75	±0.92	78843.3	±0.03	0.0012	±1.2E-05
pH=8.4 Arag. 2	142.96	±0.90	52051.3	±0.03	0.0027	±1.8E-05
pH=8.4 Arag. 4	199.57	±1.71	52489.0	±0.03	0.0038	±2.5E-05
pH=8.0 Arag. 2	65.68	±0.77	44074.7	±0.03	0.0015	±2.0E-05
pH=8.0 Arag. 3	67.47	±0.85	49190.5	±0.03	0.0014	±1.9E-05
pH=8.0 Arag. 9	63.42	±0.77	-	-	-	-
pH=8.4 Cal. 1	213.71	±1.66	46493.5	±0.03	0.0046	±2.8E-05
pH=8.4 Cal. 4	183.46	±1.34	45409.3	±0.03	0.0040	±2.6E-05
pH=8.4 Cal. 5	357.63	±4.00	45951.4	±0.03	0.0078	±4.4E-05

Table A4 (Continued) Li/Ca ratio and D_{Li} Data

pH=8.0 Cal. 4	200.20	±1.22	48531.8	±0.03	0.0041	±2.3E-05
pH=8.0 Cal. 5	115.16	±0.66	46437.7	±0.03	0.0025	±1.8E-05
1.5x[DIC] Arag. 2	112.90	±0.62	59627.8	±0.03	0.0019	±1.3E-05
1.5x[DIC] Arag. 4	124.58	±0.75	58416.0	±0.03	0.0021	±1.5E-05
0.75x[DIC] Arag. 1	155.55	±1.01	47161.3	±0.03	0.0033	±2.1E-05
0.75x[DIC] Arag. 3	219.96	±4.48	47161.3	±0.03	0.0047	±4.5E-05
1.5x[DIC] Cal. 1	239.97	±1.88	56939.5	±0.03	0.0042	±2.4E-05
1.5x[DIC] Cal. 4	131.02	±0.77	56858.4	±0.03	0.0023	±1.5E-05
0.75x[DIC] Cal. 14	142.13	±1.36	47633.2	±0.03	0.0030	±2.5E-05
0.75x[DIC] Cal. 15	153.72	±1.67	46936.0	±0.03	0.0033	±2.8E-05
0.5x[Ca ²⁺] Arag. 1	148.69	±0.92	121162.2	±0.03	0.0012	±7.9E-06
0.5x[Ca ²⁺] Arag. 5	101.67	±0.61	116825.0	±0.03	0.0009	±6.7E-06
1.5x[Ca ²⁺] Arag. 2	174.91	±1.19	33439.0	±0.03	0.0052	±3.3E-05
1.5x[Ca ²⁺] Arag. 3	153.56	±0.95	32656.9	±0.03	0.0047	±3.0E-05
1.5x[Ca ²⁺] Cal. 1	237.43	±1.93	33277.8	±0.03	0.0071	±4.2E-05
1.5x[Ca ²⁺] Cal. 3	156.92	±0.96	28004.5	±0.03	0.0056	±3.5E-05
0.5x[Ca ²⁺] Cal. 3	135.84	±1.01	113905.0	±0.03	0.0012	±8.8E-06
0.5x[Ca ²⁺] Cal. 4	139.67	±0.87	126211.8	±0.03	0.0011	±7.4E-06
0.5x[Ca ²⁺]/pH=8.4 Arag. 2	242.30	±2.12	116101.8	±0.03	0.0021	±1.3E-05
0.5x[Ca ²⁺]/pH=8.4 Arag. 3	227.28	±1.96	109529.0	±0.03	0.0021	±1.3E-05
1.5x[Ca ²⁺]/pH=8.0 Arag. 1	104.06	±0.79	31073.3	±0.03	0.0033	±2.9E-05
1.5x[Ca ²⁺]/pH=8.0 Arag. 2	107.83	±0.77	31803.1	±0.03	0.0034	±2.8E-05
0.5x[Ca ²⁺]/pH=8.4 Cal. 2	108.28	±0.76	105577.5	±0.03	0.0010	±8.2E-06
0.5x[Ca ²⁺]/pH=8.4 Cal. 4	180.75	±1.39	119249.4	±0.03	0.0015	±9.9E-06
1.5x[Ca ²⁺]/pH=8.0 Cal. 1	137.33	±0.84	24035.1	±0.03	0.0057	±3.8E-05
1.5x[Ca ²⁺]/pH=8.0 Cal. 2	130.12	±0.81	31022.5	±0.03	0.0042	±2.9E-05

Table A5: Na/Ca and Mg/Ca Data
For solution and solid samples

<u>Sample</u>	<u>Solid</u>		<u>Solution</u>	
	Mg/Ca	Na/Ca	Mg/Ca	Na/Ca
<u>Parameter/Run #</u>	<u>mmol/mol</u>	<u>mmol/mol</u>	<u>mmol/mol</u>	<u>mmol/mol</u>
Ctrl. Arag. 1	3.84	0.77	702.85	249.68
Ctrl. Arag. 2	2.97	0.44	728.55	246.69
Ctrl. Arag. 4	1.16	0.28	730.80	258.32
Ctrl. Arag. 5	-	-	700.18	245.45
Ctrl. Arag. 8	2.98	0.62	632.80	241.41
Ctrl. Arag. 9	4.46	0.20	664.30	217.54
Ctrl. Cal. 1	0.28	11.18	694.10	243.77
Ctrl. Cal. 2	-	-	702.44	249.79
Ctrl. Cal. 3	0.54	13.12	716.06	254.38
Ctrl. Cal. 4	-	-	690.49	247.67
Ctrl. Cal. 6	0.50	13.96	689.22	246.02
Ctrl. Cal. 8	4.01	12.24	709.23	264.96
Ctrl. Cal. 9	0.13	10.21	674.55	211.81
Ctrl. Cal. 11	-	-	672.69	221.38
pH=8.4 Arag. 2	6.71	1.38	613.60	261.25
pH=8.4 Arag. 4	12.79	2.69	642.90	249.49
pH=8.0 Arag. 2	11.08	1.85	563.06	248.27
pH=8.0 Arag. 3	8.97	2.01	615.42	247.49
pH=8.0 Arag. 9	8.66	1.38	551.69	272.55
pH=8.4 Cal. 1	1.49	22.46	489.58	275.85
pH=8.4 Cal. 4	0.96	21.20	505.30	255.96
pH=8.4 Cal. 5	6.01	44.53	534.85	276.99
pH=8.0 Cal. 4	0.94	39.96	498.02	254.11
pH=8.0 Cal. 5	1.57	24.83	582.55	254.35
1.5x[DIC] Arag. 2	5.56	1.69	736.69	424.05
1.5x[DIC] Arag. 4	8.25	1.97	728.43	416.40
0.75x[DIC] Arag. 1	7.32	2.21	637.57	185.72
0.75x[DIC] Arag. 3	15.52	3.69	624.89	190.74
1.5x[DIC] Cal. 1	6.59	33.59	694.42	400.85
1.5x[DIC] Cal. 4	1.40	17.27	692.51	404.94
0.75x[DIC] Cal. 14	0.84	25.60	631.93	187.69
0.75x[DIC] Cal. 15	8.46	25.02	628.33	197.34
0.5x[Ca ²⁺] Arag. 1	15.07	2.22	611.55	501.37
0.5x[Ca ²⁺] Arag. 5	6.99	1.60	632.88	502.95
1.5x[Ca ²⁺] Arag. 2	12.59	3.07	678.38	178.51
1.5x[Ca ²⁺] Arag. 3	9.99	2.36	662.72	173.32
1.5x[Ca ²⁺] Cal. 1	3.47	34.31	687.16	190.29
1.5x[Ca ²⁺] Cal. 3	0.73	22.04	-	183.52
0.5x[Ca ²⁺] Cal. 3	0.69	30.52	633.77	507.80

Table A5 (Continued): Na/Ca and Mg/Ca Data

0.5x[Ca ²⁺] Cal. 4	0.80	31.39	635.22	508.90
0.5x[Ca ²⁺]/pH=8.4 Arag. 2	14.62	3.77	540.37	523.51
0.5x[Ca ²⁺]/pH=8.4 Arag. 3	13.51	3.17	621.12	511.20
1.5x[Ca ²⁺]/pH=8.0 Arag. 1	7.72	2.59	615.96	172.39
1.5x[Ca ²⁺]/pH=8.0 Arag. 2	8.30	2.01	654.84	169.03
0.5x[Ca ²⁺]/pH=8.4 Cal. 2	0.49	17.29	630.74	501.48
0.5x[Ca ²⁺]/pH=8.4 Cal. 4	1.30	28.27	626.17	503.98
1.5x[Ca ²⁺]/pH=8.0 Cal. 1	0.66	34.15	642.76	172.24
1.5x[Ca ²⁺]/pH=8.0 Cal. 2	0.52	26.45	633.55	168.97

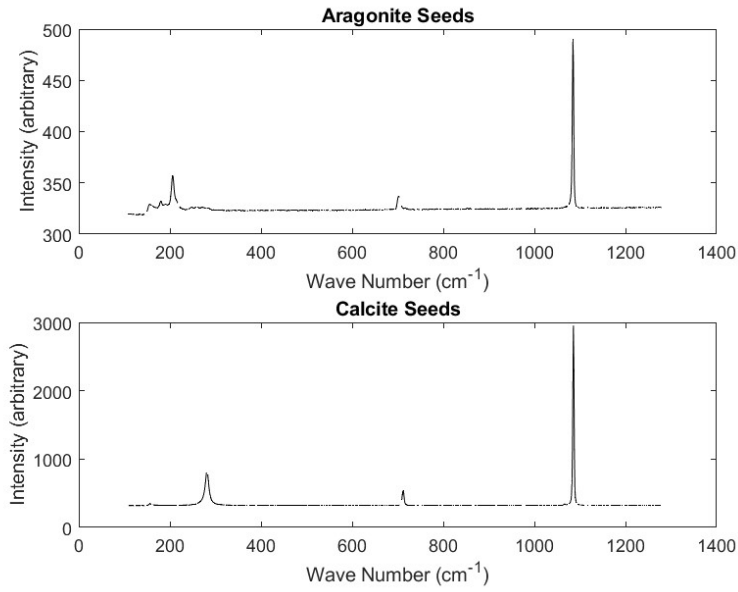


Figure A1: Raman Frequency Plots
Aragonite seeds (top) and calcite seeds (bottom).

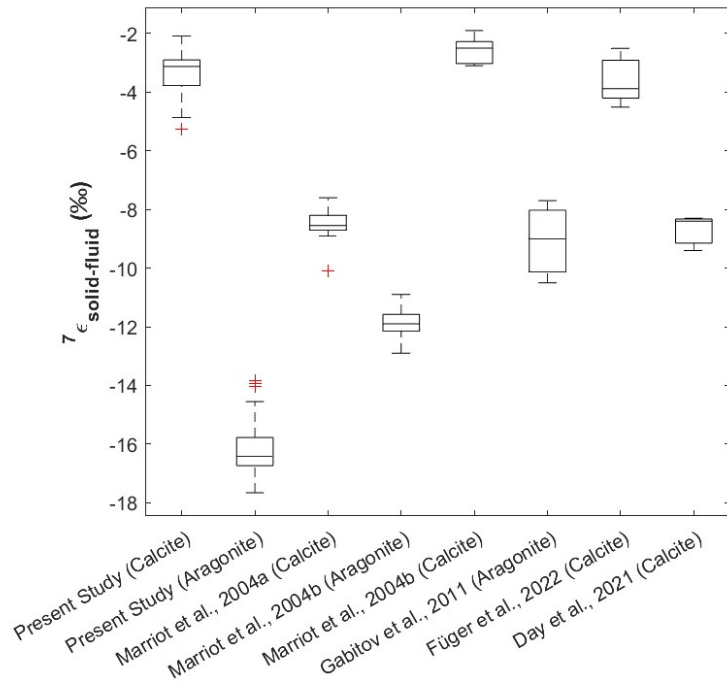


Figure A2: ${}^7\epsilon_{\text{solid-solution}}$ Across Multiple Studies
Fractionation for calcite and aragonite samples across multiple studies.

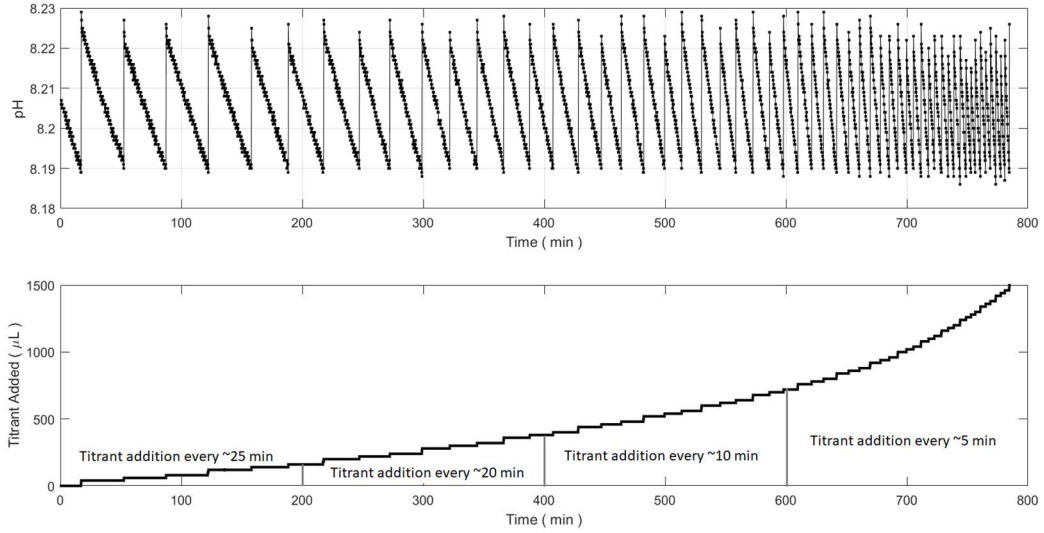


Figure A3: Titrant Addition Rate Acceleration

Titration addition plot for a control calcite precipitation experiment with average rate of titrant addition listed for ~200 min intervals. Rate of titrant addition (reflecting precipitation rate) increases by a factor of 5 from start of experiment to end of experiment.

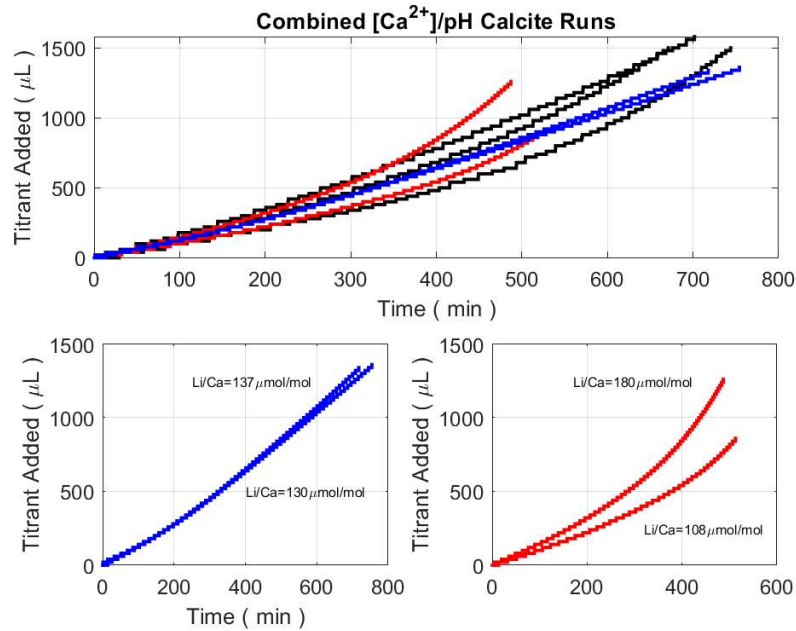


Figure A4: Titration Addition Plots for $[Ca^{2+}]/pH$ Series

In the top figure, the lines represent titrant addition and approximate precipitation rate for control runs (black), $pH = 8.0$ and $[Ca^{2+}] = 7.875$ mM (blue), and $pH = 8.4$ and $[Ca^{2+}] = 2.625$ mM (red). In the bottom two subplots, Li/Ca ratio for precipitated calcite are placed to compare with each run. For the $pH = 8.0$ and $[Ca^{2+}] = 7.875$ mM (blue), precipitation rate is steady and Li/Ca ratios are similar in value. For $pH = 8.4$ and $[Ca^{2+}] = 2.625$ mM (red), there is more variability in both rate of precipitation as well as resulting Li/Ca ratios.

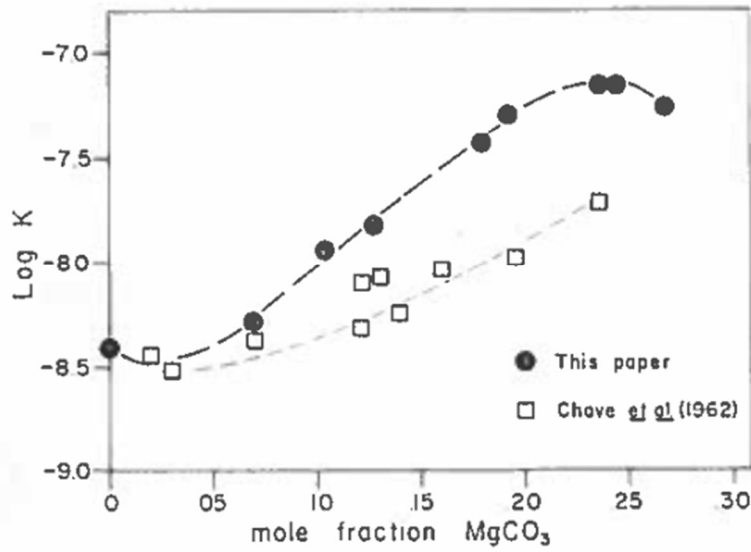


Fig A5: Mole Fraction MgCO₃ vs Log K

The mole% MgCO₃ in Mg-Calcite and the solubility constant (log K) based on studies by *Chove et al. (1962)* and *Plummer & Mackenzie (1974)*. The curve shows that with low-Mg calcite (less than 5 mole % MgCO₃), solubility decreases from pure calcite (0 mole% MgCO₃). At higher-Mg calcite levels, solubility sharply increases (greater than 5 mole % MgCO₃). (*Plummer & Mackenzie, 1974*).

References

- Allen, K.A., Hönisch, B., Eggins, S.M., Haynes, L.L., Rosenthal, Y., Yu, J. (2016). Trace element proxies for surface ocean conditions: A synthesis of culture calibrations with planktic foraminifera. *Geochim. Cosmochim. Acta*, 193. 197-221.
- Ball J. W. and Nordstrom D. K. (1991). User's manual for WATEQ4F, with revised thermodynamic data base and testcases for calculating speciation of major, trace, and redox elements in natural waters. U.S. Geological Survey Open-File Report, 91-183.
- Berner, R.A. (1975). The role of magnesium in the crystal growth of calcite and aragonite from sea water. *Geochim. Cosmochim. Acta*, 39. 489-504.
- Berner, R.A., & Caldeira, K. (1997). The need for mass balance and feedback in the geochemical carbon cycle. *Geology*, 25. 955–956.
- Bigeleisen, J. (1965). Chemistry of Isotopes. *Science.*, 147. 43-471.
- Bohlin, M., Misra, S., Lloyd, N., Elderfield, H., & Bickle, M. (2018). High-precision determination of lithium and magnesium isotopes utilising single column separation and multi-collector inductively coupled plasma mass spectrometry. *Rapid Commun. Mass Spectrom.*, 32. 93-104.
- Bots, P., Benning, L.G., Rickaby, R.E.M., & Shaw, S. (2011). The role of SO₄ in the switch from calcite to aragonite seas. *Geology*, 39(4). 331-334.
- Broecker, W., & Sanyal, A. (1998). Does atmospheric CO₂ police the rate of chemical weathering? *Global Biogeochem. Cycles*, 12. 403-408.
- Brunauer S., Emmett P. H. and Teller E. (1938). Adsorption of gases in multimolecular layers. *J. Am. Chem. Soc.*, 60. 309–319
- Busenberg, E., & Plummer, L. (1985). Kinetic and thermodynamic factors controlling the distribution of SO₄²⁻ and Na⁺ in calcites and selected aragonite. *Geochim. Cosmochim. Acta*, 49. 713-725.
- Carpenter, S. J. & Lohmann, K. C. (1992). Sr/Mg ratios of modern marine calcite: Empirical indicators of ocean chemistry and precipitation rate. *Geochim. Cosmochim. Acta*, 56. 1837–1849.
- Caves, J., Jost, A., Lau, K., & Maher, K. (2016). Cenozoic carbon cycle imbalances and a variable weathering feedback. *Earth Planet. Sci. Lett.*, 450. 152-163.
- Chan L. H., Edmond J. M., Thompson G., and Gillis K. (1992). Lithium isotopic composition of submarine basalts: Implications for the lithium cycle in the oceans. *Earth Planet. Sci. Lett.*, 108. 151–160.
- Day, C.C., Pogge von Strandmann, P.A., & Mason, A.J. (2021). Lithium isotopes and partition coefficients in inorganic carbonates: Proxy calibration for weathering reconstruction. *Geochim. Cosmochim. Acta*, 305. 243-262.
- De La Pierre, M., Carteret, C., Maschio, L., André, E., Orlando, R., & Dovesi, R. (2014). The Raman spectrum of CaCO₃ polymorphs calcite and aragonite: combined experimental and computational study. *J. Chem. Phys.*, 140. 164509

- de Nooijer, L.J., Spero, H.J., Erez, J., Bijma, J., & Reichard, G.J. (2014). Biomineralization in perforate foraminifera. *Earth Sci. Rev.*, 135. 48-58.
- Delaney, M., Bé, A., & Boyle, E. (1985). Li, Sr, Mg, and Na in foraminiferal calcite shells from laboratory culture, sediment traps, and sediment cores. *Geochim. Cosmochim. Acta*, 49. 1327-1341.
- Delaney, M., & Boyle, E. (1986). Lithium in foraminiferal shells: implications for high-temperature hydrothermal circulation fluxes and oceanic crustal generation rates. *Earth Planet. Sci. Lett.*, 80. 91-105.
- DePaolo, D.J. (2011). Surface kinetic model for isotopic and trace element fractionation during precipitation of calcite from aqueous solutions. *Geochim. Cosmochim. Acta*, 75. 1039-1056.
<https://doi.org/10.1016/j.gca.2010.11.020>.
- Erez, J. (2003). The Source of Ions for Biomineralization in Foraminifera and Their Implications for Paleoceanographic Proxies. *Reviews in Mineralogy and Geochemistry*, 54. 115-149.
- Faure, G. & Mensing, T.M. (2004). *Isotopes: Principles and Applications*. Wiley.
- Fitzsimons, I., Harte, B., & Clark, R. (2000). SIMS stable isotope measurement: Counting statistics and analytical precision. *Mineralogical Magazine*, 64(1). 59-83.
- Flesch G. D., Anderson A., Svec H. (1973). A secondary isotopic standard for $^6\text{Li}/^7\text{Li}$ determinations. *Int. J. Mass Spectrom. Ion Phys.*, 12. 265.
- Füger, A., Konrad, F., Leis, A., Dietzel, M., & Mavromatis, V. (2019). Effect of growth rate and pH on lithium incorporation in calcite. *Geochim. Cosmochim. Acta*, 248. 14-24.
- Füger, A., Kuessner, M., Rollion-Bard, C., Leis, A., Magna, T., Dietzel, M., & Mavromatis, V. (2022). Effect of growth rate and pH on Li isotope fractionation during its incorporation in calcite. *Geochim. Cosmochim. Acta*, 323. 276-290.
- Gabitov, R., Schmitt, A., Rosner, M., McKeegan, K., Gaetani, G., Cohen, A., Watson, E.B., & Harrison, T. (2011). In situ $\delta^7\text{Li}$, Li/Ca, and Mg/Ca analyses of synthetic aragonites. *Geochem. Geophys. Geosyst.*, 12. Q03001, doi:10.1029/2010GC003322.
- Geerken, E., de Nooijer, L., Toyofuku, T., Roepert, A., Middelburg, J.J., Kienhuis, M.C.M., Nagai, Y., Polerecky, L., & Reichart, G. (2022). High precipitation rates characterize biomineralization in the benthic foraminifera *Ammonia beccarii*. *Geochim. Cosmochim. Acta*, 318. 70-82.
- Gussone, N., Böhm, F., Eisenhauer, A., Dietzel, M., Heuser, A., Teichert, B.M.A., Reitner, J., Wörheid, G., & Dullo, W. (2005). Calcium isotope fractionation in calcite and aragonite. *Geochim. Cosmochim. Acta*, 69. 4485-4494.
- Hall, J., Chan, L., McDonough, W., & Turekian, K. (2005). Determination of the lithium isotopic composition of planktic foraminifera and its application as a paleo-seawater proxy. *Mar. Geol.*, 217. 255-265.
- Hathorne, E., & James, R. (2006). Temporal record of lithium in seawater: a tracer for silicate weathering? *Earth Planet. Sci. Lett.*, 246. 393-406.

- Haynes, L. L., Hönisch, B., Dyez, K. A., Holland, K., Rosenthal, Y., Fish, C. R., Subhas, A. V., & Rae, J. W. B. (2017). Calibration of the B/Ca proxy in the planktic foraminifer *Orbulina universa* to Paleocene seawater conditions, *Paleoceanography*, 32, 580–599. doi:10.1002/2016PA003069.
- Hofmann, A.E., Bourg, I.C., & DePaolo, D.J. (2012). Ion desolvation as a mechanism for kinetic isotope fractionation in aqueous systems. *Proc. Natl. Acad. Sci. U.S.A.* 109(46), 18689-18694. <https://doi.org/10.1073/pnas.1208184109>
- Holland, K., S. E. Eggins, B. Hönisch, & L. L. Haynes (2017). Calcification rate and microenvironment response of the planktic foraminifer *Orbulina universa* to changing seawater carbonate chemistry, *Earth Planet. Sci. Lett.*, 464, 124–134.
- Huh, Y., Lui-Heung, C., Zhang, L., & Edmond, J.M. (1998). Lithium and its isotopes in major world rivers: Implications for weathering and the oceanic budget. *Geochim. Cosmochim. Acta*, 62, 2039-2051.
- Jalilehvand, F., Spångberg, D., Lindqvist-Reis, P., Hermansson, K., Persson, I., & Sandström, M. (2001). Hydration of the Calcium Ion. An EXAFS, Large-Angle X-ray Scattering, and Molecular Dynamics Simulation Study. *J. Am. Chem. Soc.*, 123, 431-441.
- Juzer, S., Tanwar, N., & Misra, S. (2022). Precise determination of lithium isotope ratios at the sub-nanogram level by QQQ-ICP-MS: application to natural waters and carbonates. *J. Anal. At. Spectrom.* 37, 1541-1553.
- Lear, C., Mawbey, E., & Rosenthal, Y. (2010) Cenozoic benthic foraminiferal Mg/Ca and Li/Ca records: Toward unlocking temperatures and saturation states. *Paleoceanography*, 25, PA4215, doi:10.1029/2009PA001880.
- Lenton, T., & Britton, C. (2006). Enhanced carbonate and silicate weathering accelerates recovery from fossil fuel CO₂ perturbations. *Global Biogeochem. Cycles*, 20, GB3009, doi:10.1029/2005GB002678.
- Li, G., & West, A. (2014). Evolution of Cenozoic seawater lithium isotopes: Coupling of global denudation regime and shifting seawater sinks. *Earth. Planet. Sci. Lett.*, 401, 284-293.
- Marriott, C., Henderson, G., Crompton, R., Staubwasser, M., & Shaw, S. (2004a). Effect of mineralogy, salinity, and temperature on Li/Ca and Li isotope composition of calcium carbonate. *Chem. Geol.*, 212, 5-15.
- Marriott, C., Henderson, G., Belshaw, N., & Tudhope, A. (2004b). Temperature dependence of $\delta^7\text{Li}$, $\delta^{44}\text{Ca}$ and Li/Ca during growth of calcium carbonate. *Earth Planet. Sci. Lett.*, 222, 615-624.
- Mavromatis, V., Goetschl, K., Grengg, C., Konrad, F., Purgstaller, B., & Dietzel, M. (2018). Barium partitioning in calcite and aragonite as a function of growth rate. *Geochim. Cosmochim. Acta*, 237, 65-78.
- Misra, S., & Froelich, P. (2012). Lithium isotope history of Cenozoic seawater: changes in silicate weathering and reverse weathering. *Science*, 335, 818-823.
- Misra, S., Greaves, M., Owen, R., Kerr, J., Elmore, A. C., & Elderfield, H. (2014). Determination of B/Ca of natural carbonates by HR-ICP-MS. *Geochemistry, Geophysics, Geosystems*, 15, 1617–1628. <https://doi.org/10.1002/2013GC005049>

- Momma, K., & Izumi, F. (2011). "VESTA 3 for three-dimensional visualization of crystal, volumetric and morphology data," *J. Appl. Crystallogr.*, 44. 1272-1276.
- Morse, J., Wang, Q., & Tsio, M. (1997). Influences of temperature and Mg:Ca ratio on CaCO₃ precipitates from seawater. *Geology*, 25. 85-87.
- Morse, J.W., Arvidson, R.S., & Lüttge, A. (2007). Calcium Carbonate Formation and Dissolution. *Chem. Rev.*, 107. 342-381.
- Mucci, A. (1988). Manganese uptake during calcite precipitation from seawater: Conditions leading to the formation of a pseudokutnahorite. *Geochim. Cosmochim. Acta.*, 52. 1859-1868.
- Mucci, A., & Morse, J.W. (1983). The incorporation of Mg²⁺ and Sr²⁺ into calcite overgrowths: influences of growth rate and solution composition. *Geochim. Cosmochim. Acta.*, 47. 217-233.
- Mucci, A., Canuel, R., & Zhong, S. (1989). The solubility of calcite and aragonite in sulfate-free seawater and the seeded growth kinetics and composition of the precipitates at 25°C. *Chem. Geol.*, 74. 309-320.
- Okumura, M., & Kitano, Y. (1986). Coprecipitation of alkali metal ions with calcium carbonate. *Geochim. Cosmochim. Acta*, 50. 49-58.
- Pan, Y. Li, Y., Ma, Q., He, H., Wang, S., Sun, Z., Cai, W., Dong, B. Di, Y., Fu, W., & Chen, C.A. (2021). The role of Mg²⁺ in inhibiting CaCO₃ precipitation from seawater. *Marine Chemistry*. 237. 104036. <https://doi.org/10.1016/j.marchem.2021.104036>
- Parkhurst D. L. and Appelo C. A. J. (1999). User's guide to PHREEQC (version 2) – a computer program for speciation, batch-reaction, one-dimensional transport, and inverse geo-chemical calculations. U.S. Geological Survey, Water-Resource Investigations Report, 99-4259.
- Penniston-Dorland, S, Liu, X-M., & Rudnick, R. (2017). Lithium isotope geochemistry. *Rev. Mineral. Geochem.*, 82. 165-217.
- Plumer, L.N, & Mackenzie F.T. (1974). Predicting mineral solubility from rate data: Application to the dissolution of magnesian calcites. *Amer. J. Sci.*, 274. 61-83.
- Pogge von Strandmann, P., Jenkyns, H., & Woodfine, R. (2013). Lithium isotope evidence for enhanced weathering during Oceanic Anoxic Event 2. *Nat. Geosci.*, 6. 668-672
- Ravizza, G., & Zachos, J. (2004). Chapter 20: Records of Cenozoic Ocean Chemistry. In: *Treaties on Geochemistry (Vol. 6). The Oceans and Marine Geochemistry* (ed. H. Elderfield). Amsterdam, Elsevier. P 551-581.
- Raymo, M.E., Ruddiman, W.F., & Froelich, P.N. (1988). Influence of late Cenozoic mountain building on ocean geochemical cycles. *Geology*, 16. 649-653.
- Roberts, J., Kaczmarek, K., Langer, G., Skinner, L., Bijma, J., Bradbury, H., Turchyn, A., Lamy, F., & Misra, S. (2018). Lithium isotopic composition of benthic foraminifera: a new proxy for paleo-pH reconstruction. *Geochim. Cosmochim. Acta*, 236. 336-350.
- Romanek, C., Grossman, E., & Morse, J. (1992). Carbon isotope fractionation in synthetic aragonite and calcite: Effects of temperature and precipitation rate. *Geochim Cosmochim. Acta*, 56. 419-430.

- Sanyal A., Nugent M., Reeder R. J., & Bijma J. (2000). Seawater pH control on the boron isotopic composition of calcite: evidence from inorganic calcite precipitation experiments. *Geochim. Cosmochim. Acta*, 64. 1551–1555.
- Seyedali, M., Coogan, L.A., & Gillis, K.M. (2021). The effect of solution chemistry on elemental and isotopic fractionation of lithium during inorganic precipitation of calcite. *Geochim. Cosmochim. Acta*, 331. 102-118. doi: <https://doi.org/10.1016/j.gca.2021.07.021>
- Stewart, J., James, R., Anand, P., & Wilson, P. (2017). Silicate weathering and carbon cycle controls on the Oligocene-Miocene transition glaciation. *Paleoceanography*, 32. 1070-1085.
- Sun, H., Xiao, Y., Gao, Y., Zhang, G., Casey, J., & Shen, Y. (2018). Rapid enhancement of chemical weathering recorded by extremely light seawater lithium isotopes at the Permian-Triassic boundary. *Proc. Nat. Acad. Sci.*, 115. 3782-3787.
- Uchikawa, J., & Zeebe, R. (2008). Influence of terrestrial weathering on ocean acidification and the next glacial inception. *Geophys. Res. Lett.*, 35. L23608, doi:10.1029/2008GL035963.
- Uchikawa, J., Penman, D., Zachos, J., & Zeebe, R. (2015) Experimental evidence for kinetic effects on B/Ca in synthetic calcite: Implications for potential B(OH)₄ – and B(OH)₃ incorporation. *Geochim. Cosmochim. Acta*, 150. 171-191.
- Uchikawa, J., Harper, D., Penman, D., Zachos, J., & Zeebe, R. (2017). Influence of solution chemistry on boron content in inorganic calcite grown in artificial seawater. *Geochim. Cosmochim. Acta*, 218. 291-307.
- Vigier, N., Rollion-Bard, C., Levenson, Y., & Erez, J. (2015). Lithium isotopes in foraminifera shells as a novel proxy for the ocean dissolved inorganic carbon (DIC). *Comptes Rendus Geosci.*, 347. 43-51.
- Walker, J., Hays, P., & Kasting, J. (1981). A negative feedback mechanism for the long-term stabilization of Earth's surface temperature. *J. Geophys. Res.*, 86. 9776-9782.
- Watson E. B., & Liang Y. (1995). A simple model for sector zoning in slowly grown crystals: Implications for growth rate and lattice diffusion, with emphasis on accessory minerals in crustal rocks. *Am. Mineral.*, 80. 1179–1187.
- Watson, E.B. (2004). A conceptual model for near-surface kinetic controls on the trace-element and stable isotope composition of abiogenic calcite crystals. *Geochim. Cosmochim. Acta.*, 68. 1473-1488. doi:10.1016/j.gca.2003.10.003
- Wray, J., & Daniels, F. (1957). Precipitation of calcite and aragonite. *J. Am. Chem. Soc.*, 79. 2031-2034.
- Yamaji, K., Makita, Y., Watanabe, H., Sonoda, A., Kanoh, H., Hirotsu, T., & Ooi, K. (2001). Theoretical Estimation of Lithium Isotopic Reduced Partition Function Ratio for Lithium Ions in Aqueous Solution. *J. Phys. Chem. A.*, 105. 602-613.
- Yoder, L. (1919). Adaptation of the Mohr Volumetric Method to General Determinations of Chlorine. *Ind. Eng. Chem.*, 11. 8. 755.

Yoshimura, T., Tamenori, Y., Suzuki, A., Kawahata, H., Iwasaki, N., Hasegawa, H., Nguyen, L., Kuroyanagi, A., Yamazaki, T., Kuroda, J., & Ohkouchi, N. (2017). Altrivalent substitution of sodium for calcium in biogenic calcite and aragonite. *Geochim. Cosmochim. Acta*, 202. 21-38.

Zeebe, R., & Wolf-Gladrow, D. (2001) *CO₂ in Seawater: Equilibrium, Kinetics, Isotopes*. Elsevier Oceanography Series, Elsevier.

Zeebe, R. E. & Sanyal, A. (2002). Comparison of two potential strategies of planktonic foraminifera for house building: Mg²⁺ or H⁺ removal? *Geochim. Cosmochim. Acta*, 66. 1159–1169.

Zeebe, R., & Caldeira, K. (2008). Close mass balance of long-term carbon fluxes from ice-core CO₂ and ocean chemistry records. *Nature Geosci.*, 1. 312–315, <https://doi.org/10.1038/ngeo185>

Zeebe, R. (2012). History of seawater carbonate chemistry, atmospheric CO₂, and ocean acidification. *Annu. Rev. Earth Planet. Sci.*, 40. 141-165.

Zhang, J., Quay, P.D., & Wilbur, D.O. (1995). Carbon isotope fractionation during gas-water exchange and dissolution of CO₂. *Geochim. Cosmochim. Acta*, 59. 107-114.